Reformulating the Hoogendoorn-Bovy predictive dynamic user-optimal model in continuum space with anisotropic condition

Jie Du[1], S.C. Wong[2], Chi-Wang Shu[3], and Mengping Zhang[4]

Abstract: Hoogendoorn and Bovy (Transportation Research Part B, 2004, 38(7), 571–592) developed an approach for a pedestrian user-optimal dynamic assignment in continuous time and space. Although their model was proposed for pedestrian traffic, it can also be applied to urban cities. The model is very general, and consists of a conservation law (CL) and a Hamilton-Jacobi-Bellman (HJB) equation that contains a minimum value problem. However, only an isotropic application example was given in their paper. We claim that the HJB equation is difficult to compute numerically in an anisotropic case. To overcome this, we reformulate their model for a dense urban city that is arbitrary in shape and has multiple central business districts (CBDs). In our model, the minimum value problem is only used in the CL portion, and the HJB equation reduces to a Hamilton-Jacobi (HJ) equation for easier computation. The dynamic path equilibrium of our model is proven in a different way from theirs, and a numerical algorithm is also provided to solve the model. Finally, we show two numerical examples under the anisotropic case and compare the results with those of the isotropic case.

Key Words: Anisotropic, Continuum model, Dynamic traffic assignment, Predictive user equilibrium, Conservation law, Hamilton-Jacobi equation.

[1]School of Mathematical Sciences, University of Science and Technology of China, Hefei, Anhui, P.R. China. E-mail: dujie@mail.ustc.edu.cn

[2]Department of Civil Engineering, The University of Hong Kong, Pokfulam Road, Hong Kong, P.R. China. E-mail: hhecwsc@hku.hk

[3]Division of Applied Mathematics, Brown University, Providence, RI, USA. E-mail: shu@dam.brown.edu

[4]School of Mathematical Sciences, University of Science and Technology of China, Hefei, Anhui, P.R. China. E-mail: mpzhang@ustc.edu.cn

1 Introduction

Over recent decades, numerous traffic studies have been devoted to the modeling and numerical algorithms of the traffic equilibrium problem. A conventional methodology used in these works is the discrete modeling approach (Sheffi, 1984), in which the number of roads is finite and each road link within the network is modeled separately. This implies that the land use characteristics of several square kilometers are concentrated to a single point and served by a single strategic link. This approach is used for detailed studies of travel patterns in discrete road network systems.

In contrast, the continuum modeling approach (Buckley, 1979; Wong, 1998; Wong et al., 1998; Xiong et al., 2011; Zhang et al., 2008) focuses on the overall behavior of travelers and is thus more suitable for macroscopic studies. It approximates a dense transportation system as a continuum in which users can move freely in a continuous two-dimensional space. Hence, the continuous approach provides a more realistic representation of the network and spatially varied quantities than does the discrete approach. In the continuum modeling approach, the differences between adjacent areas within a network are assumed to be relatively small compared with the variation over the entire area, and hence the characteristics of the network, such as the flow intensity, traffic demand, density and travel cost, can be represented by smooth mathematical functions (Vaughan, 1987). Loo et al. (2005) applies the continuous modeling approach to solve large-scale airport competition and co-ordination problems in the real world and provides the modelers with valuable information about the applicability of continuum models for real-life problems.

The majority of the studies that have used the continuum modeling approach for urban cities have been confined to static cases. Because the temporal variations in the traffic characteristics are not considered in the static models, they cannot be used to handle problems such as travelers' departure/arrival time choices or dynamic traffic management and control, etc. To deal with these dynamic traffic problems and govern

the dynamic changes, dynamic traffic assignment (DTA) (Chow, 2009; Lo and Szeto, 2005) has received much attention in recent decades. The DTA literature review is vast, ranging from mathematical programming, to variational inequality, optimal control, and simulation-based. Peeta and Ziliaskopoulos (2001) give a detailed review of the existing literature.

According to the target conditions, DTA models can be classified in two groups: system optimum (SO), which aims to minimize the system's total travel cost, and dynamic user equilibrium (DUE), which aims to minimize the travel cost of each traveler. An important component of DUE is the route and departure-time choice model. Friesz et al. (1993) show a variational inequality may be used to represent DUE when there are both route and departure-time choices. Friesz et al. (2013) present a dynamic loading procedure, which determines traffic states from the link dynamics. Unlike the reactive dynamic user equilibrium (RDUE) problem, in which travelers make their choice to minimize the instantaneous travel cost and change their choice in a reactive manner (Boyce et al., 1993; Kuwahara and Akamatsu, 2001), the predictive dynamic user equilibrium (PDUE) problem assumes that travelers have perfect information about the modeled domain and choose the route that minimizes the actual travel cost (Hoogendoorn and Bovy, 2004; Lo and Szeto, 2002; Szeto and Lo, 2004; Tong and Wong, 2000).

According to the dependence of direction, the traffic equilibrium problem can be classified into two categories: isotropic problems and anisotropic problems. In isotropic problems, the traffic characteristics are uniform in all orientations. For example, the traffic speed at the same point has the same intensity regardless of the direction of the velocity vector. The local travel cost per unit distance of travel at the same point is independent of the direction of movement. Unlike in the isotropic case, anisotropic problems are used to describe situations in which properties vary systematically, dependent on the direction. In the anisotropic case, the traffic speed at the same point can be different when measured along different travel directions. The local travel cost per unit distance

of travel depends on the direction of movement.

To remedy the limitations of the discrete modeling approach, Hoogendoorn and Bovy (2004) put forward an approach for the predictive user-optimal DTA problem in continuous time and space, where traffic units (e.g. pedestrians) cannot improve their experienced utility (e.g. experienced or actual travel costs instead of instantaneous travel costs) by unilaterally changing their path choice. Contrary to the discrete approach, the traffic space is not represented as a directed graph consisting of nodes and links, but rather as a continuous plane. Their theory allows the traffic units to choose from a non-countable set of paths through the considered space at any location. This assignment model enables the prediction of future traffic conditions to minimize the actual travel cost (PDUE problem). Although their approach is primarily developed for analyzing pedestrian flow, they emphasize that travelers can also represent other types of traffic units moving in continuous space, such as ships and cars, etc. In particular, the approach can be applied to model traffic flows in dense urban cities. To the best of our knowledge, this is the first PDUE model to use the continuum modeling approach. Their model is general enough to handle both the isotropic and anisotropic cases.

Their model consists of a conservation law (CL) and a Hamilton-Jacobi-Bellman (HJB) equation. Each of CL and HJB contains a minimum value problem. For the isotropic case, the minimum value problem can be solved explicitly. However, there is no analytical solution for most anisotropic cases. In Hoogendoorn and Bovy (2004), the authors did not offer a numerical algorithm to solve the minimum value problem. In their numerical example, it is assumed that only the pedestrian density determines the maximum walking speeds, irrespective of the pedestrians' directions. Only an isotropic application example is given in their paper for the sake of simplicity.

We claim that the HJB equation is difficult to compute numerically in the anisotropic case. Hence, we reformulate their model for a dense urban city that is arbitrary in shape and has multiple central business districts (CBDs). In our model, the minimum value

problem is only used in the CL portion, and the HJB equation is reduced to a Hamilton-Jacobi (HJ) equation for more efficient computation. The minimum value problem in the CL portion is also easier to compute than that in the Hoogendoorn-Bovy model. We can solve it numerically in advance and do not need to solve it again during the model's computational process. Our model's dynamic path equilibrium is proven in a different way from theirs, and the numerical algorithm to solve the model, including the minimum value problem, is given. Finally, we provide two numerical examples under the anisotropic case and compare the results with those of the isotropic case.

The remainder of this paper is organized as follows. The description of the problem is given in the next section. In Section 3, we review the formulation of the Hoogendoorn-Bovy model. In Section 4, we discuss the reformulation of their model. We describe the solution algorithm in Section 5. In Section 6, we present two anisotropic numerical examples and compare the results with those of the isotropic case. Our conclusions are presented in Section 7.
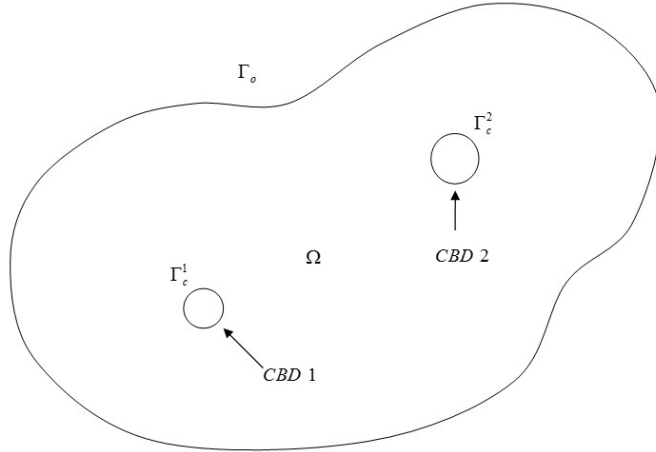
2   Problem description

Figure 1: The modeling domain

As Figure 1 shows, the modeled region is an urban city with multiple CBDs. It can

be arbitrary in shape and is denoted by Ω. Although we only plot two CBDs in Figure 1, our model is capable for the case of more than two CBDs. Let Γ_o be the outer boundary of the city and let Γ_c^m be the boundary of the mth compact CBD. Thus, the boundary of Ω is $\Gamma = \Gamma_o \cup (\cup_m \Gamma_c^m)$. The travelers' homes are continuously located along $(x, y) \in \Omega$. We assume that all of the travelers will travel to the CBDs and no traveler is allowed to leave the city by crossing the boundary Γ_o. We do not consider the destination choice in this paper and assume that the travelers of Group m travel to the mth CBD within the modeling region for a given time-dependent demand. Hence, CBDs other than the mth CBD will be viewed as obstacles for the travelers of Group m.

The variables are denoted as follows.

- $T = [0, t_{end}]$ (in h) is the time horizon.

- $q^m(x, y, t)$ (in $veh/km^2/h$) is the given travel demand of Group m at location $(x, y) \in \Omega$ at time $t \in T$, which is a non-negative and time-varying function.

- $\rho^m(x, y, t)$ (in veh/km^2) is the time-varying density of Group m at location (x, y) at time t.

- $\xi^m(x, y, t)$ is the angle between the direction of movement of Group m and the x-axis at location (x, y) at time t. We use it to represent the travel direction. It is determined by a proper path choice strategy.

- $U_f^m(x, y, t)$ is the free-flow speed of Group m. We consider the anisotropic situation in this paper, and the free-flow speed is supposed to be related to the travel direction $\xi^m(x, y, t)$ and can be computed by

$$U_f^m(x, y, t) = u_f(x, y) h(\xi^m(x, y, t)). \tag{1}$$

Here, $u_f(x, y)$ is a fixed factor to the location (x, y). $h(\xi^m(x, y, t))$ expresses that the free-flow speed along different directions may be different due to the road conditions such as major/minor road configuration.

- $U^m(x, y, t)$ is the travel speed of Group m at location (x, y) and at time t and can be determined by the free-flow speed and the total density as

$$U^m(x, y, t) = U_f^m(x, y, t)G(\sum_m \rho^m(x, y, t)). \tag{2}$$

We denote $\rho = \sum_m \rho^m$ as the total density. $G(\rho)$ is a monotonic decreasing function in ρ satisfying $G(0) = 1$. When the total density is zero, U^m reduces back to the free-flow speed. $G(\rho)$ is also supposed to vanish for density beyond a jam density ρ_{jam}. From this definition, we can see that the anisotropy of speed U^m is reflected in the free-flow speed U_f^m.

- $\mathbf{v^m}(x, y, t) = (u^m(x, y, t), v^m(x, y, t))$ is the velocity vector of Group m, where

$$u^m(x, y, t) = U^m(x, y, t) \cos\left(\xi^m(x, y, t)\right), \tag{3}$$

$$v^m(x, y, t) = U^m(x, y, t) \sin\left(\xi^m(x, y, t)\right).$$

- $\mathbf{F^m} = (f^m(x, y, t), g^m(x, y, t))$ is the flow vector of Group m, which is defined as

$$\mathbf{F^m} = \rho^m \mathbf{v^m}. \tag{4}$$

- $|\mathbf{F^m}|$ is the flow intensity of Group m, which is the norm of the flow vector $\mathbf{F^m}$, and is defined as

$$|\mathbf{F^m}| = \rho^m U^m. \tag{5}$$

- $c^m(x, y, t)$ (in $\$/km$) is the local travel cost of traveling one unit of distance along $\mathbf{v^m}$ at location (x, y) at time t. It is defined as

$$c^m(x, y, t) = \kappa(\frac{1}{U^m} + \pi(\sum_m \rho^m)). \tag{6}$$

where κ is the value of time, $\frac{\kappa}{U^m}$ represents the cost associated with the travel time, and $\kappa\pi(\sum_m \rho^m)$ represents other costs that are dependent of the total density. If we consider the cost associated with the travel time, then we have

$$c^m(x, y, t) = \frac{\kappa}{U^m}, \tag{7}$$

because the speed U^m is an anisotropic variable, $c^m(x, y, t)$ is also anisotropic; that is, the travel cost of moving one unit of distance is related to the direction of movement.

- $\phi^m(x, y, t)$ is the actual total travel cost incurred by a traveler who departs from location (x, y) at time t to travel to the mth CBD using the constructed path-choice strategy.

- $\varphi^m(x, y, t)$ is the angle between $-\nabla \phi^m$ and the x-axis, where $\nabla = (\frac{\partial}{\partial x}, \frac{\partial}{\partial y})$.

- $\mathbf{n}(x, y)$, $(x, y) \in \Gamma$ is the unit outward normal vector on the boundary.

Next, we construct a path-choice strategy under the anisotropic assumption and a model of this problem to govern these variables. Here, we assume that the road network is very dense and that travelers can move freely in it. We also assume that travelers have full and perfect information about traffic conditions over time, and that they will therefore choose the path that minimizes the actual travel cost (not the instantaneous travel cost), resulting in a predictive user equilibrium for a dynamic system.

3 The Hoogendoorn-Bovy dynamic user-optimal model

In this section, we briefly review the Hoogendoorn-Bovy dynamic user-optimal model and show the difficulty in solving the HJB equation. For consistency, we have changed the notations in their formulation to match ours.

Using our notations, the Hoogendoorn-Bovy dynamic user-optimal model can be written as

$$\begin{cases} -\phi_t^m = \min_{\tilde{\mathbf{v}}}\{L(x, y, t, \tilde{\mathbf{v}}) + \tilde{\mathbf{v}} \cdot \nabla \phi^m\}, \\ \rho_t^m + \nabla \cdot (\rho^m \mathbf{v^m}) = q^m(x, y, t), \\ \mathbf{v^m} = arg \min\{L(x, y, t, \tilde{\mathbf{v}}) + \tilde{\mathbf{v}} \cdot \nabla \phi^m\}, \end{cases} \tag{8}$$

with some proper initial boundary conditions. Here, L is the so-called running cost. It reflects the cost incurred during one unit time period. $\tilde{\mathbf{v}}(x, y, t) = (\tilde{u}(x, y, t), \tilde{v}(x, y, t))$ is any possible velocity vector at point (x, y) at time t. $\mathbf{v^m}$ is the optimal velocity vector

of Group m. For simplicity, we omit the superscript m in the following discussion when there is no confusion.

The whole model consists of two coupled partial differential equations (PDEs). The first equation in their model is an HJB or dynamic programming equation, which includes a minimum value problem. The HJB equation typically arises in an optimal control problem and is a result of dynamic programming theory (Bellman, 1957). The following numerical scheme (Fleming and Soner, 1993) is used to solve this equation:

$$\phi_{i,j}^{n-1} = \phi_{i,j}^n - \Delta t \hat{H}((\phi_x)_{i,j}^{n,-}, (\phi_x)_{i,j}^{n,+}, (\phi_y)_{i,j}^{n,-}, (\phi_y)_{i,j}^{n,+}), \tag{9}$$

with the numerical Hamiltonian $\hat{H}$ defined by

$$\hat{H} = \min_{\tilde{\mathbf{v}}} \{ L(x, y, t, \tilde{\mathbf{v}}) + \tilde{u}^+ (\phi_x)_{i,j}^{n,+} + \tilde{u}^- (\phi_x)_{i,j}^{n,-} + \tilde{v}^+ (\phi_y)_{i,j}^{n,+} + \tilde{v}^- (\phi_y)_{i,j}^{n,-} \}. \tag{10}$$

Here,

$$w^+ = \max\{w, 0\}, \qquad w^- = \min\{w, 0\}. \tag{11}$$

$$(\phi_x)_{i,j}^{n,+} = \frac{\phi_{i+1,j}^n - \phi_{i,j}^n}{\Delta x}, \qquad (\phi_x)_{i,j}^{n,-} = \frac{\phi_{i,j}^n - \phi_{i-1,j}^n}{\Delta x}, \tag{12}$$

are the forward and backward finite differences in the x-axis.

$$(\phi_y)_{i,j}^{n,+} = \frac{\phi_{i,j+1}^n - \phi_{i,j}^n}{\Delta y}, \qquad (\phi_y)_{i,j}^{n,-} = \frac{\phi_{i,j}^n - \phi_{i,j-1}^n}{\Delta y}, \tag{13}$$

are the finite differences in the y-axis. The second equation of their model is a CL. In this equation, $\mathbf{v}$ is the optimal velocity vector solved by the same minimum value problem; that is,

$$\mathbf{v} = arg \min_{\tilde{\mathbf{v}}} \{ L(x, y, t, \tilde{\mathbf{v}}) + \tilde{u}^+ (\phi_x)_{i,j}^{n,+} + \tilde{u}^- (\phi_x)_{i,j}^{n,-} + \tilde{v}^+ (\phi_y)_{i,j}^{n,+} + \tilde{v}^- (\phi_y)_{i,j}^{n,-} \}. \tag{14}$$

In Hoogendoorn and Bovy (2004), the authors use an iteration procedure to solve these two coupled equations. In each iteration, the HJB equation and the CL are calculated once for each group of travelers, respectively. Hence, the minimum value problem must be solved twice for each group of travelers at each numerical point in an iteration.

Note that to achieve the stability of the numerical scheme for the HJB equation, the wind direction must be considered in the numerical scheme of the minimum value problem. The partial derivatives must be replaced with appropriate finite differences. When $\tilde{u} > 0$, the forward finite difference $(\phi_x)_{i,j}^+$ is used to approximate ϕ_x. When $\tilde{u} < 0$, we use the backward finite difference $(\phi_x)_{i,j}^-$ to approximate ϕ_x. Similarly, the numerical method used to approximate ϕ_y is determined by the sign of $\tilde{v}$. The final numerical scheme is influenced by the sign of the optimal velocity $\mathbf{v}$, which is an unknown value to be solved. In most anisotropic cases, the explicit relations between the optimal velocity and the minimum actual route cost can not be found. Actually, there are infinite $\tilde{\mathbf{v}}$ to be chosen, and it is difficult to solve the optimal one. In Hoogendoorn and Bovy (2004), the authors do not provide a numerical procedure to solve this minimum value problem. Because the wind direction is considered, both $\tilde{u}$ and $\tilde{v}$ are split into positive and negative portions, and hence the scheme of the minimum value problem is not smooth with respect to $\tilde{\mathbf{v}}$. In addition to the unknown value $\tilde{\mathbf{v}}$, there are five parameters—L, $(\phi_x)_{i,j}^+$, $(\phi_x)_{i,j}^-$, $(\phi_y)_{i,j}^+$ and $(\phi_y)_{i,j}^-$—which differ from the varied numerical points and iterations. All of these problems increase the complexity of constructing a numerical procedure to solve this minimum value problem.

In our reformulation of the model, we show how to compute the actual total travel cost ϕ when the velocity vector in the time-space domain is known. In this case, the equation to solve ϕ reduces to an HJ equation, which includes no minimum value problem and hence is much easier to solve. The minimum value problem to solve the optimal velocity vector is only used in the CL portion. Hence, we only need to solve the minimum value problem one time for each group of travelers in each iteration. Moreover, the sign of the optimal velocity vector $\mathbf{v}$ dose not influence the numerical scheme used to solve the CL. Because ϕ is supposed to be known when solving the CL, we do not need to consider the wind direction of ϕ when approximating ϕ_x and ϕ_y in solving the minimum value problem. In other words, we do not need to use the numerical scheme (14) in which $\tilde{u}$

and $\tilde{v}$ are split into positive and negative portions. The numerical scheme for our model is smooth with respect to $\tilde{\mathbf{v}}$. As we show in Section 5, because we do not need to use different finite differences to approximate ϕ_x and ϕ_y, there is only one parameter left in the minimum value problem when the cost is only related to the travel time. Hence, we can discretize the range of this parameter into many discrete points and solve the minimum value problem numerically in advance at each point. Therefore, we do not need to solve the minimum value problem again during the model's computational process; we need only read the result at the closest discrete point. This method is difficult to extend to solve the minimum value problem in the Hoogendoorn-Bovy model because there are still four parameters—$(\phi_x)_{i,j}^+$, $(\phi_x)_{i,j}^-$, $(\phi_y)_{i,j}^+$ and $(\phi_y)_{i,j}^-$—even when the time is related only to the time.

4 Reformulation of the Hoogendoorn-Bovy model

In this section, we reformulate the Hoogendoorn-Bovy model. In Section 4.1, we derive the HJ equation to compute $\phi^m(x, y, t)$ with any given velocity vector $(u^m(x, y, t), v^m(x, y, t))$ in the time-space domain. In Section 4.2, we give the CL to solve $\rho^m(x, y, t)$ and illustrate the path-choice strategy to choose the optimal velocity vector capable of minimizing the actual total travel cost. A proof of the dynamic user equilibrium is given in the path-choice strategy. We discuss the initial and boundary conditions of the HJ and CL in Section 4.3. We conclude the complete formulation of our new model in Section 4.4 and illustrate how to formulate it as a fixed-point problem.

4.1 The derivation of the HJ equation to compute the actual total cost $\phi^m(x, y, t)$

We use the time-space domain in our discussion, as shown in Figure 2. We use the x-y plane to represent the space domain in which the vehicles drive. The vertical axis represents the time. Let the coordinate of point A in the x-y plane be (x, y). The curve that passes the point (x, y, t) represents the 3D trajectory of a vehicle passing point A

at time t and heading toward the destination in the time-space domain.
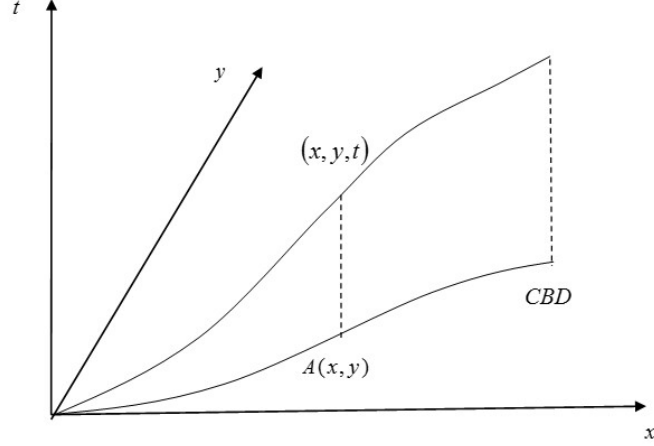

Figure 2: The 3D trajectory of a vehicle

We now illustrate how to compute the actual total travel cost $\phi^m(x, y, t)$ when the traffic situation of Group m in the city is known. Let us define the path in the time-space domain as $(x(t), y(t), t)$ with the parameter t. When the velocity vector $\big(u^m(x, y, t), v^m(x, y, t)\big)$ is given, we have

$$\frac{dx}{dt} = u^m(x(t), y(t), t) \qquad \frac{dy}{dt} = v^m(x(t), y(t), t). \qquad (15)$$

Hence, we have

$$
\begin{aligned}
\frac{d\phi^m}{dt}(x(t), y(t), t) &= \phi_x^m \frac{dx(t)}{dt} + \phi_y^m \frac{dy(t)}{dt} + \phi_t^m \\
&= \phi_x^m u^m + \phi_y^m v^m + \phi_t^m. \qquad (16)
\end{aligned}
$$

From the definition of the derivative, we also know that

$$
\begin{aligned}
\frac{d\phi^m}{dt} &= \lim_{\Delta t \to 0} \frac{\phi^m\big(x(t+\Delta t), y(t+\Delta t), t+\Delta t\big) - \phi^m\big(x(t), y(t), t\big)}{\Delta t} \\
&= \lim_{\Delta t \to 0} -U^m \frac{\phi^m\big(x(t), y(t), t\big) - \phi^m\big(x(t+\Delta t), y(t+\Delta t), t+\Delta t\big)}{\Delta t U^m}, \qquad (17)
\end{aligned}
$$

where $U^m = \sqrt{(u^m)^2 + (v^m)^2}$ is the speed of the given velocity vector. Note that when Δt is small enough, the motion of the travelers can be viewed as uniform. Hence,

12

$\Delta t U^m$ is the distance between the points $\big(x(t), y(t)\big)$ and $\big(x(t + \Delta t), y(t + \Delta t)\big)$, and $\phi^m\big(x(t), y(t), t\big) - \phi^m\big(x(t + \Delta t), y(t + \Delta t), t + \Delta t\big)$ is the cost of traveling between these two points. Therefore, the fraction in the last equation in (17) is actually the local cost c^m and Equation (17) can be translated as

$$\frac{d\phi^m}{dt} = -U^m c^m. \tag{18}$$

By combining Equations (16) and (18) , we obtain the HJ equation to solve the cost potential ϕ^m:

$$\phi_t^m + \phi_x^m u^m + \phi_y^m v^m = -U^m c^m. \tag{19}$$

Because $u^m = U^m \cos \xi^m$, $v^m = U^m \sin \xi^m$, we have

$$\phi_t^m + \phi_x^m U^m \cos \xi^m + \phi_y^m U^m \sin \xi^m = -U^m c^m. \tag{20}$$

We provide the initial boundary conditions of this equation in Section 4.3.

4.2 Path-choice strategy

We first illustrate that all of the traffic variables can be computed, provided that the traveling directions $\xi^m(x, y, t)$ of each group in the time-space domain are given for any $(x, y) \in \Omega$ and $t \in T$. Considering the conservation of mass in fluid dynamics, the density $\rho^m(x, y, t)$ is governed by the following CL:

$$\rho_t^m + (\rho^m u^m)_x + (\rho^m v^m)_y = q^m, \qquad \forall (x, y) \in \Omega, t \in T. \tag{21}$$

Using the definitions in Section 2, we know that u^m and v^m can be expressed in terms of the total density ρ and the given ξ^m:

$$u^m(x, y, t) = u_f(x, y) h(\xi^m(x, y, t)) G(\sum_m \rho^m) \cos \big(\xi^m(x, y, t)\big), \tag{22}$$

$$v^m(x, y, t) = u_f(x, y) h(\xi^m(x, y, t)) G(\sum_m \rho^m) \sin \big(\xi^m(x, y, t)\big).$$

13

When $\xi^m(x, y, t)$ for all groups are given, we can obtain $\rho^m(x, y, t)$ by solving Eqs. (21) and (22) for each m with some proper initial boundary conditions. Then, we can obtain $\left(u^m(x, y, t), v^m(x, y, t)\right)$ using Eq. (22). Moreover, the speed $U^m(x, y, t)$ and the local cost $c^m(x, y, t)$ can be computed. Hence, we can get the resulting total actual cost $\phi^m(x, y, t)$ by solving the HJ equation.

In the above, $\xi^m(x, y, t)$ can be arbitrary. In this section, we show how to choose the optimal path direction $\xi^m(x, y, t)$ such that the predictive dynamic user equilibrium is satisfied. Here, the predictive dynamic user equilibrium is defined as,

"If, for any travellers between any OD pair leaving their origin at any instant, the actual travel times that these travellers experienced on any used routes are equal and minimal; and the actual travel times that theses travellers would experience on any unused routes are greater than or equal to the minimum actual travel time on used routes." (Tong and Wong, 2000)

From now on, we suppose that $\xi^m(x, y, t)$ denotes the optimal path direction and that all of the other variables without the superscript "$\sim$" denote the resulting traffic variables computed with $\xi^m(x, y, t)$.

For any fixed $(x_0, y_0) \in \Omega$ and $t_0 \in T$, consider a vehicle of any group (say Group m) that departs (x_0, y_0) at time t_0 along a path with an arbitrary travel angle $\tilde{\xi}$. If $\tilde{\xi} = \xi^m(x_0, y_0, t_0)$, we call this path the "used" path. If $\tilde{\xi} \neq \xi^m(x_0, y_0, t_0)$, we call this path an "unused" path. Using the definitions in Section 2, we know that the travel speed of this vehicle at (x_0, y_0, t_0) is

$$\tilde{U}^m(\tilde{\xi}) = u_f(x_0, y_0)h(\tilde{\xi})G(\sum_m \rho^m(x_0, y_0, t_0)). \tag{23}$$

Hence, the velocity vector of this vehicle at (x_0, y_0, t_0) is $\tilde{\mathbf{v}}^m(\tilde{\xi}) = (\tilde{u}^m(\tilde{\xi}), \tilde{v}^m(\tilde{\xi}))$ defined by

$$\tilde{u}^m(\tilde{\xi}) = \tilde{U}^m(\tilde{\xi}) \cos(\tilde{\xi}), \tag{24}$$
$$\tilde{v}^m(\tilde{\xi}) = \tilde{U}^m(\tilde{\xi}) \sin(\tilde{\xi}),$$

and the local travel cost of moving one unit distance along $\tilde{\xi}$ is

$$\tilde{c}^m(\tilde{\xi}) = \kappa(\frac{1}{\tilde{U}^m(\tilde{\xi})} + \pi(\sum_m \rho^m(x_0, y_0, t_0))). \qquad (25)$$

Define

$$p^m(x_0, y_0, t_0, \tilde{\xi}) = \phi_x^m(x_0, y_0, t_0)\tilde{u}^m(\tilde{\xi}) + \phi_y^m(x_0, y_0, t_0)\tilde{v}^m(\tilde{\xi}) + \tilde{c}^m(\tilde{\xi})\tilde{U}^m(\tilde{\xi}). \qquad (26)$$

From Equation (19), we know that when $\tilde{\xi} = \xi^m(x_0, y_0, y_0)$, we have

$$p^m(x_0, y_0, t_0, \xi^m(x_0, y_0, y_0)) + \phi_t^m(x_0, y_0, y_0) = 0. \qquad \forall(x_0, y_0) \in \Omega, \forall t_0 \in T. \qquad (27)$$
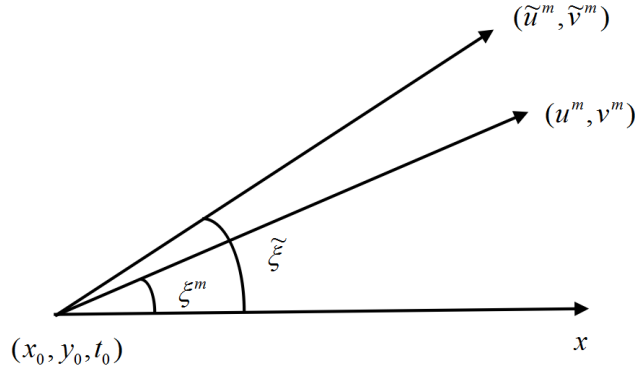
Figure 3: The "used" and "unused" paths

We now present the path-choice strategy.

Theorem 1: *If each group choose the path direction $\xi^m(x, y, t)$ such that the resulting traffic variables satisfy $p^m(x_0, y_0, t_0, \xi^m(x_0, y_0, t_0)) \leq p^m(x_0, y_0, t_0, \tilde{\xi}), \forall \tilde{\xi} \neq \xi^m(x_0, y_0, t_0),$ for all $(x_0, y_0) \in \Omega$ and $t_0 \in T$, then the dynamic predictive user equilibrium is satisfied.*

Proof: Consider a vehicle of any group m at the point (x_0, y_0, t_0). The total cost of getting to the mth CBD on the "used" path is $\phi^m(x_0, y_0, t_0)$. Define the total cost along an "unused" path as $\tilde{\phi}^m$. We need to prove that $\tilde{\phi}^m$ is no less than $\phi^m(x_0, y_0, t_0)$. We can prove this using the following two steps.

15

Step 1. Let us first consider an "unused" path with angel $\tilde{\xi}$ that deviates from the utilized path only in the first Δt time, and then reverts back to the "used" path. Here, we assume that Δt is small enough that $\phi^m(x, y, t)$ can be treated as a linear function of x and y in such a small area.

The cost in the first Δt time is

$$\tilde{c}^m(\tilde{\xi})\tilde{U}^m(\tilde{\xi})\Delta t. \tag{28}$$

Let $(\tilde{x}, \tilde{y})$ be the position at which the vehicle arrives in Δt time with the vector $\Delta t \tilde{\mathbf{v}}^m$. Because we assume that the traveler reverts back to the "used" path after the first Δt time, the travel cost from $(\tilde{x}, \tilde{y})$ to the CBD is $\phi^m(\tilde{x}, \tilde{y}, t_0 + \Delta t)$.

As we assume that ϕ^m is a linear function in such a small area, we have

$$\phi^m(\tilde{x}, \tilde{y}, t_0 + \Delta t) - \phi^m(x_0, y_0, t_0)$$
$$= (\phi_x^m, \phi_y^m, \phi_t^m) \cdot (\tilde{u}^m, \tilde{v}^m, 1)\Delta t$$
$$= (\phi_x^m \tilde{u}^m + \phi_y^m \tilde{v}^m + \phi_t^m)\Delta t. \tag{29}$$

Hence, we can obtain

$$\tilde{\phi}^m = \phi^m(\tilde{x}, \tilde{y}, t_0 + \Delta t) + \tilde{c}^m(\tilde{\xi})\tilde{U}^m(\tilde{\xi})\Delta t$$
$$= \phi^m(\tilde{x}, \tilde{y}, t_0 + \Delta t) - \phi^m(x_0, y_0, t_0) + \phi^m(x_0, y_0, t_0) + \tilde{c}^m(\tilde{\xi})\tilde{U}^m(\tilde{\xi})\Delta t$$
$$= \phi^m(x_0, y_0, t_0) + [p^m(x_0, y_0, t_0, \tilde{\xi}) + \phi_t^m]\Delta t$$
$$\geq \phi^m(x_0, y_0, t_0) + [p^m(x_0, y_0, t_0, \xi^m(x_0, y_0, t_0)) + \phi_t^m(x_0, y_0, t_0)]\Delta t$$
$$= \phi^m(x_0, y_0, t_0). \tag{30}$$

The last equality is from Equation (27).

Step 2. In the above case, if a vehicle of any group m moves along $\tilde{\xi}$ only in the first Δt period, it will arrive at the mth CBD with a cost $\tilde{\phi}^m \geq \phi^m(x_0, y_0, t_0)$. However, if it does not revert back to the "used" path in the next step and continues to move in a direction other than that of the speed vector, then by the same token it will arrive at

the mth CBD with a cost $\tilde{\tilde{\phi}}^m \geq \tilde{\phi}^m \geq \phi^m(x_0, y_0, t_0)$. Therefore, for any "unused" path, the total cost must be no less than that of the "used" path. $\square$

Note that by taking a special condition that $h(\tilde{\xi}) = 1$, our anisotropic model will reduce back to Du et al. (2013) model where the free-flow speed is isotropic. In this case, the speed intensity and the local travel cost are independent of the travel direction $\tilde{\xi}$:

$$\tilde{U}^m = U^m = u_f(x_0, y_0)G(\sum_m \rho^m(x_0, y_0, t_0)), \tag{31}$$

$$\tilde{c}^m = c^m = \kappa(\frac{1}{U^m} + \pi(\sum_m \rho^m(x_0, y_0, t_0))). \tag{32}$$

Hence, we have

$$
\begin{aligned}
p^m(x_0, y_0, t_0, \tilde{\xi}) &= \phi_x^m(x_0, y_0, t_0)\tilde{u}^m(\tilde{\xi}) + \phi_y^m(x_0, y_0, t_0)\tilde{v}^m(\tilde{\xi}) + \tilde{c}^m\tilde{U}^m \\
&= -|\nabla\phi^m|U^m \cos(\tilde{\xi} - \varphi^m) + c^m U^m \\
&\geqslant -|\nabla\phi^m|U^m + c^m U^m.
\end{aligned}
\tag{33}
$$

Obviously, we have

$$\xi^m = arg\min_{\tilde{\xi}} p^m(x_0, y_0, t_0, \tilde{\xi}) = \varphi^m, \tag{34}$$

which means that we should choose the $(u^m, v^m) \parallel (-\phi_x^m, -\phi_y^m)$. This result is exactly the same as the path choice strategy in Du et al. (2013).

4.3 The discussion of initial boundary conditions

In this section, we discuss the initial boundary conditions of the CL and HJ equations to make them a complete model.

Because we assume that travelers of Group m can not leave the city and will enter the mth CBD only, the outer boundary of the city (Γ_o) and the boundaries of CBDs other than the mth CBD ($\Gamma_c^n, n \neq m$) will be viewed as solid walls for Group m. We let the normal flow intensity of Group m be zero on these solid walls, that is

$$\mathbf{F^m}(x, y, t) \cdot \mathbf{n}(x, y) = 0, \forall(x, y) \in \Gamma_o \cup (\cup_{n \neq m}\Gamma_c^n), \quad t \in T, \tag{35}$$

where $\mathbf{n}$ is the outward unit normal vector of the solid wall.

We set the initial time as $t = 0$ and let $\rho_0^m(x, y)$ be the density of Group m at location (x, y) at the beginning of the modeling period. As such, the initial condition of CL is

$$\rho^m(x, y, 0) = \rho_0^m(x, y), \qquad \forall (x, y) \in \Omega. \tag{36}$$

For the boundary condition of HJ, we let ϕ_{CBD}^m represent the boundary value of ϕ^m on Γ_c^m, which can be interpreted as the cost to the traveler of entering the mth CBD. Now we consider the initial condition. Note that the travel cost to the CBD only depends on the events that will occur in the future, and has nothing to do with events that happened in the past. Hence, it seems reasonable to solve the HJ equation along the negative time direction.

Denote $\phi_0^m(x, y)$ as the value of ϕ^m at $t = t_{end}$. Now, we show how to compute it. Here, we assume that the travelers of all groups have entered the CBDs and that there is no traffic in the city at $t = t_{end}$. This can be considered as a static state, i.e., $(\phi_0^m)_t = 0$. The travel cost ϕ_0^m to the mth CBD is the instantaneous cost at $t = t_{end}$. Because the total density is zero everywhere at $t = t_{end}$, the speed is just the free-flow speed and the local travel cost is related to the travel time:

$$\begin{cases} U_0^m(x, y) = u_f(x, y)h(\xi_0^m(x, y)), & \forall (x, y) \in \Omega, \quad t \in T, \\ c_0^m(x, y) = \frac{\kappa}{U_0^m}, & \forall (x, y) \in \Omega, \quad t \in T. \end{cases} \tag{37}$$

Here, $\xi_0^m(x, y)$ is the optimal travel angle. By using the path-choice strategy and letting density be zero, we have

$$\xi_0^m(x, y) = \arg\min_{\tilde{\xi}} p_0^m(x, y, \tilde{\xi}) = \arg\min (\phi_0^m)_x \tilde{u}_0^m(\tilde{\xi}) + (\phi_0^m)_y \tilde{v}_0^m(\tilde{\xi}) + \kappa, \tag{38}$$

with

$$\begin{cases} \tilde{u}_0^m(\tilde{\xi}) = u_f(x, y)h(\tilde{\xi})\cos(\tilde{\xi}), \\ \tilde{v}_0^m(\tilde{\xi}) = u_f(x, y)h(\tilde{\xi})\sin(\tilde{\xi}). \end{cases} \tag{39}$$

Following the derivation in Section 4.1, we can obtain the equation to solve $\phi_0^m(x, y)$:

$$(\phi_0^m)_x U_0^m \cos \xi_0^m + (\phi_0^m)_y U_0^m \sin \xi_0^m = -\kappa, \qquad \forall (x, y) \in \Omega. \tag{40}$$

18

4.4 The complete model and fixed-point problem

In the above sections, we know that we can compute the density ρ^m using the CL and then compute the total actual travel cost ϕ^m using the HJ, provided that the travel angle $\xi^m(x, y, t)$ used in the CL is given for all groups and all points in the time-space domain. Once we know the cost ϕ^m, we can adjust the optimal $\xi^m(x, y, t)$ in the computation of CL using the path choice strategy in Theorem 1. Hence, the whole model consists of the CL and HJ portions. We conclude that our model can be written as follows.

The CL portion is

$$
\begin{cases}
\rho_t^m + (\rho^m U^m \cos \xi^m)_x + (\rho^m U^m \sin \xi^m)_y = q^m, & \forall (x, y) \in \Omega, \quad t \in T, \\
U^m(x, y, t) = u_f(x, y) h(\xi^m(x, y, t)) G(\sum_m \rho^m), & \forall (x, y) \in \Omega, \quad t \in T, \\
\xi^m(x, y, t) = arg\ \min_{\tilde{\xi}} p^m(x, y, t, \tilde{\xi}), & \forall (x, y) \in \Omega, \quad t \in T, \\
\mathbf{F^m}(x, y, t) \cdot \mathbf{n}(x, y) = 0, & \forall (x, y) \in \Gamma_o \cup (\cup_{n \neq m} \Gamma_c^n), \quad t \in T, \\
\rho^m(x, y, 0) = \rho_0^m(x, y), & \forall (x, y) \in \Omega.
\end{cases}
\tag{41}
$$

The HJ portion is

$$
\begin{cases}
\phi_t^m + \phi_x^m U^m \cos \xi^m + \phi_y^m U^m \sin \xi^m = -U^m c^m, & \forall (x, y) \in \Omega, \quad t \in T, \\
c^m = \kappa(\frac{1}{U^m} + \pi(\sum_m \rho^m)), & \forall (x, y) \in \Omega, \quad t \in T, \\
\phi^m(x, y, t) = \phi_{CBD}^m, & \forall (x, y) \in \Gamma_c^m, \quad t \in T, \\
\phi^m(x, y, t_{end}) = \phi_0^m(x, y), & \forall (x, y) \in \Omega,
\end{cases}
\tag{42}
$$

where ϕ_0^m is solved by

$$
\begin{cases}
(\phi_0^m)_x U_0^m \cos \xi_0^m + (\phi_0^m)_y U_0^m \sin \xi_0^m = -\kappa, & \forall (x, y) \in \Omega, \\
U_0^m(x, y) = u_f(x, y) h(\xi_0^m(x, y)), & \forall (x, y) \in \Omega, \\
\xi_0^m(x, y) = arg\ min_{\tilde{\xi}}\ p_0^m(x, y, \tilde{\xi}), & \forall (x, y) \in \Omega, \\
\phi_0^m(x, y) = \phi_{CBD}^m, & \forall (x, y) \in \Gamma_c^m.
\end{cases}
\tag{43}
$$

Note that the two parts of the model are closely interconnected. When solving the CL, we assume that $\phi^m(x, y, t)$ from the HJ portion is known for all m, and thus we can obtain $\xi^m(x, y, t)$ by solving the minimum value of p^m, thereby obtaining the velocity vector. When solving the HJ, we need the value of the density ρ^m to obtain the local cost. However, neither ρ^m nor ϕ^m is known in advance, and they cannot be solved together as they have different computation directions in time. Next, we show that we can compute these two parts as a fixed-point problem.

Define the vector of the numerical solutions of each group at each grid point and each time level as

$$\vec{\rho} = \{(\rho^m)_{i,j}^n, i = 1, \cdots, N_x, j = 1, \cdots, N_y, n = 1, \cdots, N_t, m = 1, \cdots, N_m\},$$
$$\vec{\phi} = \{(\phi^m)_{i,j}^n, i = 1, \cdots, N_x, j = 1, \cdots, N_y, n = 1, \cdots, N_t, m = 1, \cdots, N_m\},$$

(44)

where N_x, N_y and N_t are the numbers of grid points in x, y and t, respectively, and N_m is the number of groups. Let us now give the definition for **one iteration**. With a given vector $\vec{\phi}^{old}$, we solve the CL for each group from $t = 0$ to $t = t_{end}$ and thus can obtain a vector of density. Then we use this vector to solve the HJ equation for each group from $t = t_{end}$ to $t = 0$ to obtain an updated vector $\vec{\phi}^{new}$. We call the procedure for getting $\vec{\phi}^{new}$ from $\vec{\phi}^{old}$ as one iteration and denote it as

$$\vec{\phi}^{new} = \mathbf{f}(\vec{\phi}^{old}).$$

(45)

With the definition of one iteration and the function $\mathbf{f}$, the model translates to the problem

$$\vec{\phi} = \mathbf{f}(\vec{\phi}),$$

(46)

which is called a fixed-point problem.

5 Solution algorithm

In this section, we describe the solution algorithms to solve the reformulated model.

5.1 Solution algorithm for the minimum value problem

When solving the CL of Group m, we need to know the travel angle $\xi^m(x, y, t)$. For this purpose, we need to solve a minimum value problem $\xi^m(x, y, t) = arg\,min_{\tilde{\xi}}\, p^m(x, y, t, \tilde{\xi})$ at each numerical solution point during the computation of CL. In general, it is difficult to give an explicit expression of ξ^m. However, if we only consider the special case in which the cost is only related to the travel time, the problem can be simplified. We provide the algorithm to solve it in this section.
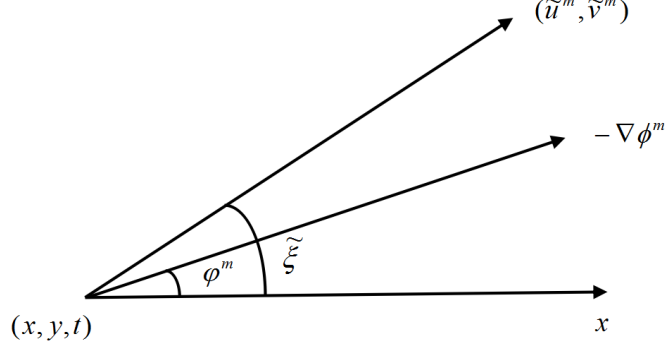
Figure 4: $\tilde{\xi}$ and φ^m

When the cost is only the time, we have $\tilde{c}^m(\tilde{\xi}) = \frac{\kappa}{\tilde{U}^m(\tilde{\xi})}$. Hence, $p^m(x,y,t,\tilde{\xi})$ becomes

$$p^m(x,y,t,\tilde{\xi})$$

$$= \nabla\phi^m \cdot \tilde{\mathbf{v}}^m(\tilde{\xi}) + \kappa$$

$$= -|\nabla\phi^m|\tilde{U}^m(\tilde{\xi})\cos(\tilde{\xi} - \varphi^m) + \kappa$$

$$= -|\nabla\phi^m|u_f(x,y)h(\tilde{\xi})G(\rho)\cos(\tilde{\xi} - \varphi^m) + \kappa$$

$$= -ah(\tilde{\xi})\cos(\tilde{\xi} - \varphi^m) + \kappa. \tag{47}$$

For any fixed point (x,y,t) in the time-space domain, we know that $a = |\nabla\phi^m|u_f(x,y)G(\rho)$ is non-negative. Hence, we have

$$\xi^m(x,y,t) = arg\,min_{\tilde{\xi}}\{p^m(x,y,t,\tilde{\xi})\} = arg\,max_{\tilde{\xi}}\{h(\tilde{\xi})\cos(\tilde{\xi} - \varphi^m)\}. \tag{48}$$

In this way, we can transform the minimum value problem into a maximum value problem and there is only one parameter φ^m.

In the numerical computation of CL, we know the value of ϕ^m and thus can obtain φ^m by

$$\cos\varphi^m = -\frac{\phi_x^m}{|\nabla\phi^m|}, \quad \sin\varphi^m = -\frac{\phi_y^m}{|\nabla\phi^m|}. \tag{49}$$

Here, we do not need to consider the wind direction of ϕ^m and can approximate ϕ_x^m and ϕ_x^m simply using

$$(\phi_x^m)_{i,j}^n \approx \frac{(\phi^m)_{i+1,j}^n - (\phi^m)_{i-1,j}^n}{2\Delta x}, \qquad (\phi_y^m)_{i,j}^n \approx \frac{(\phi^m)_{i,j+1}^n - (\phi^m)_{i,j-1}^n}{2\Delta y}, \tag{50}$$

where $(\phi^m)_{i,j}^n$ is the numerical approximation of ϕ^m at grip point (x_i, y_j) and at time level t^n. Now, we need to get ξ^m by solving the maximum value point of $h(\tilde{\xi})\cos(\tilde{\xi} - \varphi^m)$ and compute $\sin \xi^m$ and $\cos \xi^m$ to compute the conservation law.

We now divide the range of φ^m, i.e., $[0, 2\pi]$ into N sets. We define $\varphi_i = \frac{2\pi}{N}i, i = 0, 1, \cdots, N$. For each $\varphi_i, i = 1 \cdots, N$, we can solve the maximum value point of $h(\tilde{\xi})\cos(\tilde{\xi} - \varphi_i)$ numerically and get the corresponding result $\xi_i, i = 1, \cdots, N$. In our numerical example, we take $N = 400000$. Before we start to compute the model, we perform the above computation and save the series $\{\xi_i, i = 1, \cdots, N\}$. When solving the CL, we just need to compute φ^m at each point and find the cell containing it. If $\varphi_j \leqslant \varphi^m < \varphi_{j+1}$, then we take $\xi^m = \xi_j$. In this way, we do not need to solve the minimum value problem during the computation of CL.

5.2 Lax-Friedrichs scheme used to solve the conservation law

In this subsection, we assume that the cost potential function $\phi^m(x, y, t)$ is known for all $(x, y) \in \Omega$ and $t \in T$. Hence, we can obtain ξ^m by the algorithm described in the above section. Now, we focus on the numerical method to solve the conservation law:

$$\rho_t^m + (\rho^m U^m \cos \xi^m)_x + (\rho^m U^m \sin \xi^m)_y = q^m. \tag{51}$$

We use the numerical solution $(\rho^m)_{i,j}^n$ to approximate the point value of $\rho^m(x_i, y_j, t^n)$. For simplicity, we omit the superscript m in the following where there is no confusion. We use a conservative difference scheme to solve CL:

$$\rho_{i,j}^{n+1} = \rho_{i,j}^n - \frac{\Delta t}{\Delta x}(\hat{f}_{i+\frac{1}{2},j} - \hat{f}_{i-\frac{1}{2},j}) - \frac{\Delta t}{\Delta y}(\hat{g}_{i,j+\frac{1}{2}} - \hat{g}_{i,j-\frac{1}{2}}) + q_{i,j}^n \Delta t, \tag{52}$$

where $q_{i,j}^n = q^m(x_i, y_j, t^n)$ is the given demand at location (x_i, y_j) at time t^n, Δx and Δy are the mesh sizes in the x and y directions, respectively and $\hat{f}_{i+\frac{1}{2},j}$ and $\hat{g}_{i,j+\frac{1}{2}}$ are numerical fluxes in the x and y directions, respectively. Here, we use the Lax-Friedrichs flux, which is a monotone flux:

$$\hat{f}_{i+\frac{1}{2},j} = \frac{1}{2}[f(\rho_{i,j}^n) + f(\rho_{i+1,j}^n) - \alpha_f(\rho_{i+1,j}^n - \rho_{i,j}^n)] \tag{53}$$

22

$$\hat{g}_{i,j+\frac{1}{2}} = \frac{1}{2}[g(\rho_{i,j}^n) + g(\rho_{i,j+1}^n) - \alpha_g(\rho_{i,j+1}^n - \rho_{i,j}^n)], \tag{54}$$

where $f(\rho) = \rho u^m$, $g(\rho) = \rho v^m$, $\alpha_f = \max |f'(\rho)|$ and $\alpha_g = \max |g'(\rho)|$. Note that the optimal traveling direction solved by the minimum value problem does not influence the numerical scheme used to solve the CL.

5.3 Lax-Friedrichs scheme used to solve the Hamilton-Jacobi portion

In this subsection, we suppose that the density $\rho^m(x, y, t)$ and the travel angle $\xi^m(x, y, t)$ are known for all $(x, y) \in \Omega$ and $t \in T$ from the CL portion, and focus on the numerical method to solve the Hamilton-Jacobi equation:

$$\begin{cases} \phi_t^m + \phi_x^m U^m \cos \xi^m + \phi_y^m U^m \sin \xi^m = -U^m c^m, & \forall (x, y) \in \Omega, \quad t \in T, \\ \phi^m(x, y, t) = \phi_{CBD}^m, & \forall (x, y) \in \Gamma_c^m, \quad t \in T, \\ \phi^m(x, y, t_{end}) = \phi_0^m(x, y), & \forall (x, y) \in \Omega. \end{cases} \tag{55}$$

Note that the value of $\phi_0^m(x, y)$ is computed by a static HJ equation. We deal with the problem later, but now we assume that $\phi_0^m(x, y)$ is known.

As we need to solve the HJ backwards in time, we define

$$\tau = t_{end} - t, \quad \Phi(x, y, \tau) = \phi^m(x, y, t_{end} - \tau), \tag{56}$$

and thus can rewrite the time-dependent HJ equation into a usual form:

$$\begin{cases} \Phi_\tau - \Phi_x U^m \cos \xi^m - \Phi_y U^m \sin \xi^m = U^m c^m, & \forall (x, y) \in \Omega, \quad \tau \in T, \\ \Phi(x, y, \tau) = \phi_{CBD}^m, & \forall (x, y) \in \Gamma_c^m, \quad \tau \in T, \\ \Phi(x, y, 0) = \phi_0^m(x, y), & \forall (x, y) \in \Omega. \end{cases} \tag{57}$$

If we define

$$H(\Phi_x, \Phi_y) = -U^m(\Phi_x \cos \xi^m + \Phi_y \sin \xi^m + c^m), \tag{58}$$

then the scheme to solve $\Phi_\tau + H(\Phi_x, \Phi_y) = 0$ is

$$\Phi_{i,j}^{n+1} = \Phi_{i,j}^n - \Delta t \hat{H}((\Phi_x)_{i,j}^{n,-}, (\Phi_x)_{i,j}^{n,+}, (\Phi_y)_{i,j}^{n,-}, (\Phi_y)_{i,j}^{n,+}), \tag{59}$$

with

$$(\Phi_x)_{i,j}^{n,-} = \frac{\Phi_{i,j}^n - \Phi_{i-1,j}^n}{\Delta x}, \qquad (\Phi_x)_{i,j}^{n,+} = \frac{\Phi_{i+1,j}^n - \Phi_{i,j}^n}{\Delta x}, \tag{60}$$

$$(\Phi_y)_{i,j}^{n,-} = \frac{\Phi_{i,j}^n - \Phi_{i,j-1}^n}{\Delta y}, \qquad (\Phi_y)_{i,j}^{n,+} = \frac{\Phi_{i,j+1}^n - \Phi_{i,j}^n}{\Delta y}, \qquad (61)$$

where $\hat{H}$ is a Lipschitz continuous monotone flux consistent with H. Here, we use the global Lax-Friedrichs flux:

$$\hat{H}(u^-, u^+, v^-, v^+) = H\left(\frac{u^- + u^+}{2}, \frac{v^- + v^+}{2}\right) - \frac{1}{2}\alpha^x(u^+ - u^-) - \frac{1}{2}\alpha^y(v^+ - v^-), \quad (62)$$

where α^x and α^y are defined as

$$\alpha^x = \max_{A \leq u \leq B, C \leq v \leq D} |H_1(u, v)|, \qquad \alpha^y = \max_{A \leq u \leq B, C \leq v \leq D} |H_2(u, v)|. \qquad (63)$$

H_1 (H_2) is the partial derivative of H in terms of Φ_x (Φ_y), $[A, B]$ is the value range of $u^{\pm}$ and $[C, D]$ is the value range of $v^{\pm}$.

Now, we deal with the equation for $\phi_0^m(x, y)$:

$$\begin{cases} (\phi_0^m)_x U_0^m \cos \xi_0^m + (\phi_0^m)_y U_0^m \sin \xi_0^m = -\kappa, & \forall (x, y) \in \Omega, \\ U_0^m(x, y) = u_f(x, y) h(\xi_0^m(x, y)), & \forall (x, y) \in \Omega, \\ \xi_0^m(x, y) = arg\,min_{\tilde{\xi}}\, p_0^m(x, y, \tilde{\xi}), & \forall (x, y) \in \Omega, \\ \phi_0^m(x, y) = \phi_{CBD}^m, & \forall (x, y) \in \Gamma_c^m. \end{cases} \qquad (64)$$

This is a static HJ equation. We solve it using the method of pseudo time iterations. We reformulate the equation into the following time-dependent problem

$$\begin{cases} \Phi_t - \Phi_x U^m \cos \xi^m - \Phi_y U^m \sin \xi^m = \kappa, & \forall (x, y) \in \Omega, \quad t \geqslant 0, \\ U^m(x, y, t) = u_f(x, y) h(\xi^m(x, y, t)), & \forall (x, y) \in \Omega, \quad t \geqslant 0, \\ \xi^m(x, y, t) = arg\,min_{\tilde{\xi}}\, p_0^m(x, y, \tilde{\xi}), & \forall (x, y) \in \Omega, \quad t \geqslant 0, \\ \Phi(x, y, t) = \phi_{CBD}^m, & \forall (x, y) \in \Gamma_c^m, \quad t \geqslant 0, \\ \Phi(x, y, 0) = 10^{12}, & \forall (x, y) \in \Omega/\Gamma_c^m, \end{cases} \qquad (65)$$

by setting a large value as the initial guess. Now, we perform the same Lax-Friedrichs technique described above to find the steady-state solution of this time-evolving equation. At each time level, we need to solve the minimum value problem using the updated Φ. Finally, we set the converged solution of this time-dependent problem as ϕ_0^m.

Note that the computation of ϕ_0^m is independent of ρ^m because we assume $\rho^m = 0$ at time t_{end}. Hence, $\phi_0^m(x, y)$ is fixed for each $(x, y) \in \Omega$. We only need to solve ϕ_0^m once at the beginning of the whole computation procedure of the model and read them again when needed.

5.4 A self-adaptive MSA to solve the fixed-point problem

As illustrated in Section 4.4, our model can be viewed as a fixed-point problem $\vec{\phi} = \mathbf{f}(\vec{\phi})$. It can be solved by a self-adaptive method of successive averages (MSA). We proposed this method in Du et al. (2013) to solve the PDUE problem under isotropic assumption. We briefly introduce this method in this section for the completeness of this paper. For more details, we refer to Du et al. (2013).

The MSA was first introduced by Robbins and Monro (1951) to solve the fixed-point problem. A general MSA is an iterative process. If we denote the solution before the kth iteration as $\vec{\phi}^k$, then computing the MSA to obtain $\vec{\phi}^{k+1}$ involves the following steps:

Step 1. Solve a temporary solution $\vec{y}^k = \mathbf{f}(\vec{\phi}^k)$ during the kth iteration.

Step 2. Choose a step size λ_k and use the following equation to obtain $\vec{\phi}^{k+1}$:

$$\vec{\phi}^{k+1} = (1 - \lambda_k)\vec{\phi}^k + \lambda_k \cdot \vec{y}^k, \ k = 1, 2, \cdots \tag{66}$$

Convergence is declared if

$$\|\vec{\phi}^{k+1} - \vec{\phi}^k\| \leq \delta, \tag{67}$$

where δ is a given convergence threshold value. We use $\delta = 10^{-2}$ and L^2 as the norm in our computation.

The choice of the step size $\{\lambda_k\}$ is important to the convergence speed of MSA. Bar-Gera and Boyce (2006) constructed a type of MSA with a constant step size sequence, efficiently solving travel forecasting problems. With the assumption that $\mathbf{f}$ is smooth enough and the Jacobi matrix of $\mathbf{f}$ can be diagonalized by a orthonormal matrix, Bar-Gera and Boyce (2006) derived the following formula:

$$\frac{\|\vec{\phi}^{k+1} - \mathbf{f}(\vec{\phi}^{k+1})\|^2}{\|\vec{\phi}^k - \mathbf{f}(\vec{\phi}^k)\|^2} \to r^*(\lambda), \tag{68}$$

where λ is the constant step size and $r^*(\lambda)$ is a convex quadratic function that is pointing up. In addition, $r^*(0) = 1$ and $\frac{\partial r^*}{\partial \lambda}(0) < 0$. Any constant step size such that $r^*(\lambda) < 1$ results in convergence. There specially exists an optimal constant step size $0 < \lambda^* \leq 1$

such that $r^*(\lambda^*) = \min_\lambda r^*(\lambda)$. However, because the constant step size is related to the properties of $\mathbf{f}(\vec{\phi})$, this method needs to estimate the optimal step size according to past experience and decrease it as necessary. Bar-Gera and Boyce (2006) didn't offer a general method for determining the optimal constant step size for different problems.

Based on Formula (68), we proposed a self-adaptive MSA in Du et al. (2013) to automatically determine the optimal MSA step size without prior information. Although the convergence of this method depends on the property of the mapping $\mathbf{f}$, it works very well in Du et al. (2013). We also use it in this paper. The procedure for determining the optimal step size used in the self-adaptive MSA is as follows.

1. For the first several iterations, we use the predetermined step sizes

$$\lambda_1 = 1.0, \lambda_2 = 0.4, \lambda_3 = 0.3, \lambda_4 = 0.2, \lambda_5 = 0.15, \lambda_6 = 0.1, \lambda_7 = 0.05. \qquad (69)$$

2. After the kth iteration ($k > 2$), we record the step size λ_{k-1} used before this iteration and the resulting ratio of the error

$$r_{k-1} = \frac{\|\vec{\phi}^k - \mathbf{f}(\vec{\phi}^k)\|^2}{\|\vec{\phi}^{k-1} - \mathbf{f}(\vec{\phi}^{k-1})\|^2}, \qquad (70)$$

thus constituting a discrete point (λ_{k-1}, r_{k-1}) to fit the curve $r^*(\lambda)$.

3. For the $n + 1(n \geq 7)$ step size, we use the least squares method to fit the discrete points $(\lambda_k, r_k), k = 2, \cdots, n$ and obtain a fitted quadratic curve $r^*(\lambda)$. We require this curve to pass through the point $(0, 1)$, and as such only two parameters must be determined to fit the curve. Define the new step size λ_{n+1} as the minimum point of $r^*(\lambda)$, i.e., $r^*(\lambda_{n+1}) = \min_\lambda r^*(\lambda)$.

4. If the new step size is invalid, such that $\lambda_{n+1} \leq 0$ or $\lambda_{n+1} \geq 1$, then we abandon it and set $\lambda_{n+1} = 0.5\lambda_n$.
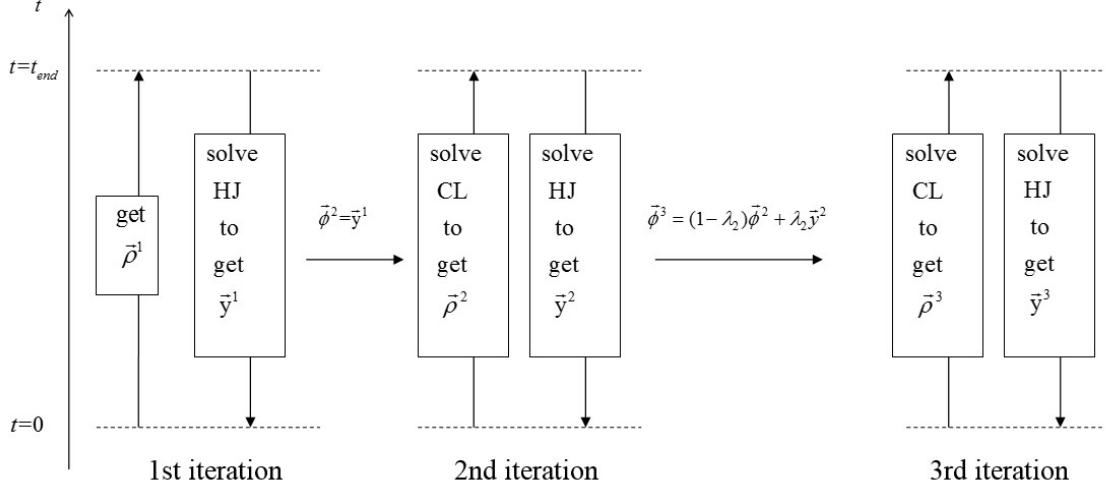
Figure 5: Solution procedure

5.5 Solution procedure

To start the self-adaptive MSA, we explain how to compute the first iteration. At the beginning of the MSA, we have no information about the actual total cost of traveling to the CBDs. When we solving the CL, we approximate ϕ^m by the instantaneous total cost to the destination at each time level and suppose that the travel direction is parallel to $-\nabla\phi^m$. We compute the instantaneous total cost at each time level by using $|\nabla\phi^m| = c^m(x, y, t)$. This formulation is derived in Huang et al., 2009. Hence, we can compute the density $\rho^m(x, y, t)$ by solving the following model for each group:

$$\begin{cases} \rho_t^m + (\rho^m U^m \cos\xi^m)_x + (\rho^m U^m \sin\xi^m)_y = q^m, & \forall(x, y) \in \Omega, \quad t \in T, \\ U^m(x, y, t) = u_f(x, y)h(\xi^m(x, y, t))G(\sum_m \rho^m), & \forall(x, y) \in \Omega, \quad t \in T, \\ \cos\xi^m = -\frac{\phi_x^m}{|\nabla\phi^m|}, \, \sin\xi^m = -\frac{\phi_y^m}{|\nabla\phi^m|}, & \forall(x, y) \in \Omega, \quad t \in T, \\ |\nabla\phi^m| = c^m(x, y, t), & \forall(x, y) \in \Omega, \quad t \in T, \end{cases} \tag{71}$$

subject to the initial boundary conditions

$$\begin{cases} \mathbf{F^m}(x, y, t) \cdot \mathbf{n}(x, y) = 0, & \forall(x, y) \in \Gamma_o \cup (\cup_{n \neq m}\Gamma_c^n), \quad t \in T, \\ \rho^m(x, y, 0) = \rho_0^m(x, y), & \forall(x, y) \in \Omega, \\ \phi^m(x, y, t) = \phi_{CBD}^m, & \forall(x, y) \in \Gamma_c^m, \quad t \in T. \end{cases} \tag{72}$$

We denote the density vector solved by this equation as $\vec{\rho}^1$. We can then solve the HJ Equation (42) to obtain $\vec{y}^1$, and set $\vec{\phi}^2 = \vec{y}^1$.

The solution procedure is as follows.

27

1. Compute the density $\vec{\rho}^1$ from $t = 0$ to $t = t_{end}$ by solving Equation (71) for each group. Then use it to compute the HJ Equation (42) from $t = t_{end}$ to $t = 0$ for each group and obtain $\vec{y}^1$. Hence, we obtain $\vec{\phi}^2 = (1 - \lambda_1)\vec{\phi}^1 + \lambda_1 \vec{y}^1 = \vec{y}^1$.

2. Use the kth solution vector $\vec{\phi}^k$ to complete the kth iteration, $k = 2, \cdots$, i.e.,

$$\vec{y}^k = \mathbf{f}(\vec{\phi}^k). \tag{73}$$

3. Compute the step size $\lambda_k(k > 7)$ using the method described in Section 5.4. The step sizes $\lambda_k, k = 1, \cdots, 7$ are predetermined.

4. Compute the $(k + 1)$th solution vector

$$\vec{\phi}^{k+1} = (1 - \lambda_k)\vec{\phi}^k + \lambda_k \cdot \vec{y}^k. \tag{74}$$

5. Stop the iteration process when $\|\vec{\phi}^{k+1} - \vec{\phi}^k\| \leq \delta$ is satisfied.

At the end of this section, we conclude the major differences between the algorithms for this paper and Du et al. (2013). The main difficulty of solving the anisotropic problem is that we do not have an explicit expression of the optimal velocity direction ξ^m in the path-choice strategy. During the computation of the CL, we need to compute φ^m with the given value ϕ^m first and then get the corresponding ξ^m by solving a minimum value problem at each gird point and each time level. While in Du et al. (2013), we do not need to solve the minimum value problem because we already know $\xi^m = \varphi^m$ from the path choice strategy under the isotropic assumption. For the computation of ϕ_0^m in this paper, we need to solve Equation (43) by using iterative method. For each iteration, we also need to solve the minimum value problem at each grid to obtain the traveling direction. When the speed is isotropic, the traveling direction is parallel to $-\nabla \phi_0^m$ and hence Equation (43) reduces to a very simple Eikonal equation $|\nabla \phi_0^m| = c^m(x, y, t_{end})$ which contains no minimum value problem and is solved by an efficient method called fast sweeping method in Du et al. (2013). Hence, the existing scheme for isotropic case

in Du et al. (2013) is simpler and cannot be used to solve the anisotropic problem in this paper.

6 Numerical examples

To demonstrate the effectiveness of the reformulated model and the proposed algorithm for solving it, we present two anisotropic numerical examples in this section. In Section 6.1, we show a numerical example with a single CBD and compare the results with the isotropic case. In Section 6.2, we show a numerical example with two CBDs. Here, we assume that the cost is only related to the travel time so that the minimum value problem is easy to compute.

6.1 Single CBD

6.1.1 Problem setting
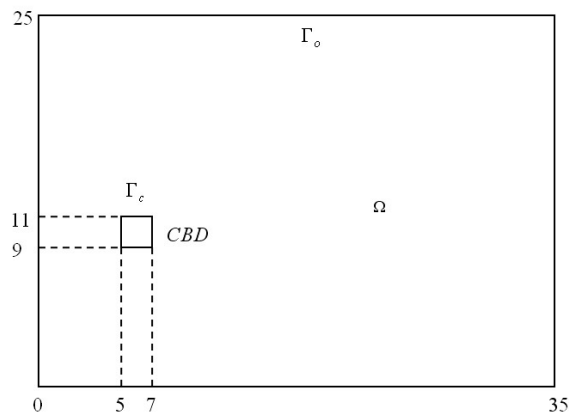
Figure 6: The modeling domain

We consider a rectangular computational domain with a single destination as shown in Figure 6. The city is 35 km long and 25 km wide. The center of the CBD is located at (6 km, 10 km). We omit the superscript m of all functions because there is only one group in this example.

We assume that there is no traffic at the beginning of the modeling period, i.e.,

29

$\rho_0(x, y) = 0, \forall(x, y) \in \Omega$, and that no cost is incurred by entering the CBD ($\phi_{CBD} = 0, \forall(x, y) \in \Gamma_c, t \in T$). The traffic demand function q is

$$q(x, y, t) = q_{max}[1 - \gamma_1 d(x, y)]s(t), \tag{75}$$

where $q_{max} = 1200veh/km^2/h$ is the maximum demand, $\gamma_1 = 0.01km^{-1}$ is a positive scalar and $d(x, y) = \sqrt{(x - 6)^2 + (y - 10)^2}$ is the distance from location (x, y) to the center of the CBD. The factor $[1 - \gamma_1 d(x, y)]$ is used to express the higher traffic demand generated in the domain closer to the CBD, where more of the population is located. $s(t)$ is a non-negative and time-varying function defined by

$$s(t) = \begin{cases} t, & t \in [0h, 1h], \\ 1, & t \in [1h, 2h], \\ -\frac{4}{5}(t - 3) + \frac{1}{5}, & t \in [2h, 3h], \\ \frac{1}{5}, & t \in [3h, 5h], \\ 0, & t \in [5h, t_{end}]. \end{cases} \tag{76}$$

We set $t_{end} = 7$ and so the modeling period is $T = [0h, 7h]$.

The free-flow speed is defined as $U_f(x, y, t) = u_f(x, y)h(\xi(x, y, t))$ with

$$u_f(x, y) = U_{max}[1 + \gamma_2 d(x, y)], \tag{77}$$

and

$$h(\xi(x, y, t)) = [\cos(2\xi) + 5]/6, \tag{78}$$

where $U_{max} = 30km/h$ and $\gamma_2 = 4 \times 10^{-3}km^{-1}$. The factor $[1 + \gamma_2 d(x, y)]$ is used to express the faster free-flow speed in the domain far from the CBD, where there are fewer junctions. The factor $[\cos(2\xi) + 5]/6$ is used to express the faster free-flow speed in the east-west direction (see Figure 7).

We define the speed function as $U(x, y, t) = U_f(x, y, t)G(\rho)$, where $G(\rho)$ is defined as

$$G(\rho) = \begin{cases} e^{-\beta(\rho)^2} - e^{-\beta(10000)^2}\frac{\rho}{10000}, & if \ \rho \leqslant 10000, \\ 0, & if \ \rho > 10000. \end{cases} \tag{79}$$

Here, $\beta = \frac{1}{32 \times 1000^2}$ (in km^4/veh^2) is a positive scalar related to the road condition. We can see that the speed decreases as the density increases and the traffic gets stuck when ρ exceeds the jam density 10000.

30
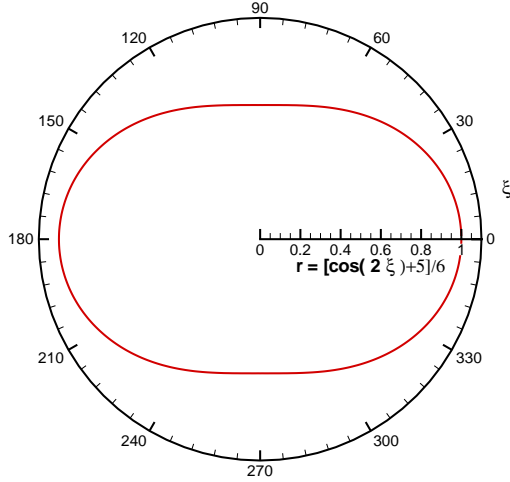
Figure 7: Polar line: $[\cos(2\xi) + 5]/6$

The flow intensity can be computed as

$$|\mathbf{F}| = \rho U = \rho U_f G(\rho). \tag{80}$$

Here, the free-flow speed $U_f(x, y, t) = u_f(x, y)h(\xi(x, y, t))$ dependents on both the location (x, y) and the travel direction ξ. For any fixed (x, y) and ξ, the flow intensity is a function of ρ only. When the density is small, $|\mathbf{F}|$ grows as ρ increases and the traffic is in a non-congested condition. When ρ exceeds a critical density $\rho_c \approx 4000$, the traffic becomes congested and $|\mathbf{F}|$ decreases as ρ increases. $|\mathbf{F}|$ reaches the maximum value at ρ_c. Note that the critical density remains the same at different locations and with different travel directions.

In the general case, the local travel cost per unit of distance is defined as

$$c(x, y, t) = \kappa(\frac{1}{U} + \pi(\rho)), \tag{81}$$

where $\kappa = 90\$/h$ and $\pi(\rho) = 10^{-8}\rho^2$. When the cost is only the travel time, we have

$$c(x, y, t) = \frac{\kappa}{U}. \tag{82}$$

A uniform rectangular mesh with an $N_x \times N_y$ grid is used in the computation. The

31

mesh grids inside the CBD are not computed. The numerical boundary conditions are summarized as follows.

1. On the solid wall boundaries, i.e., the outer boundary of the city, Γ_o, we let the normal numerical flux be 0. We set $\rho = 0$ at the ghost points inside the wall. In the HJ equation, the numerical boundary values of ϕ are obtained by extrapolation from inside the computational domain.

2. On the boundary of the compact CBD, i.e., Γ_c, we set $\phi = 0$ in the HJ equation. The boundary conditions for ρ inside the CBD are obtained by extrapolation from the grids outside the CBD. We assume that the capacity of the CBD is large enough to accommodate all of the travelers in the city. To maintain the maximum flow intensity on the boundary of the CBD under the congested condition, we set $U(x, y, t) = U_f$ inside the CBD.

6.1.2 Numerical results

We present the numerical results in this section. To verify the convergence of the composed algorithm, we test three grids (grid 1: 140×100; grid 2: 280×200; grid 3: 420×300). The one-dimensional cuts of the density at time $t = 2$ along different lines are plotted in Figure 8, which shows good convergence among different grids. Grid 2 is adopted for further discussion.

(a) $x = 7$

(b) $x = 12$

(c) $y = 10$

(d) $y = 12$
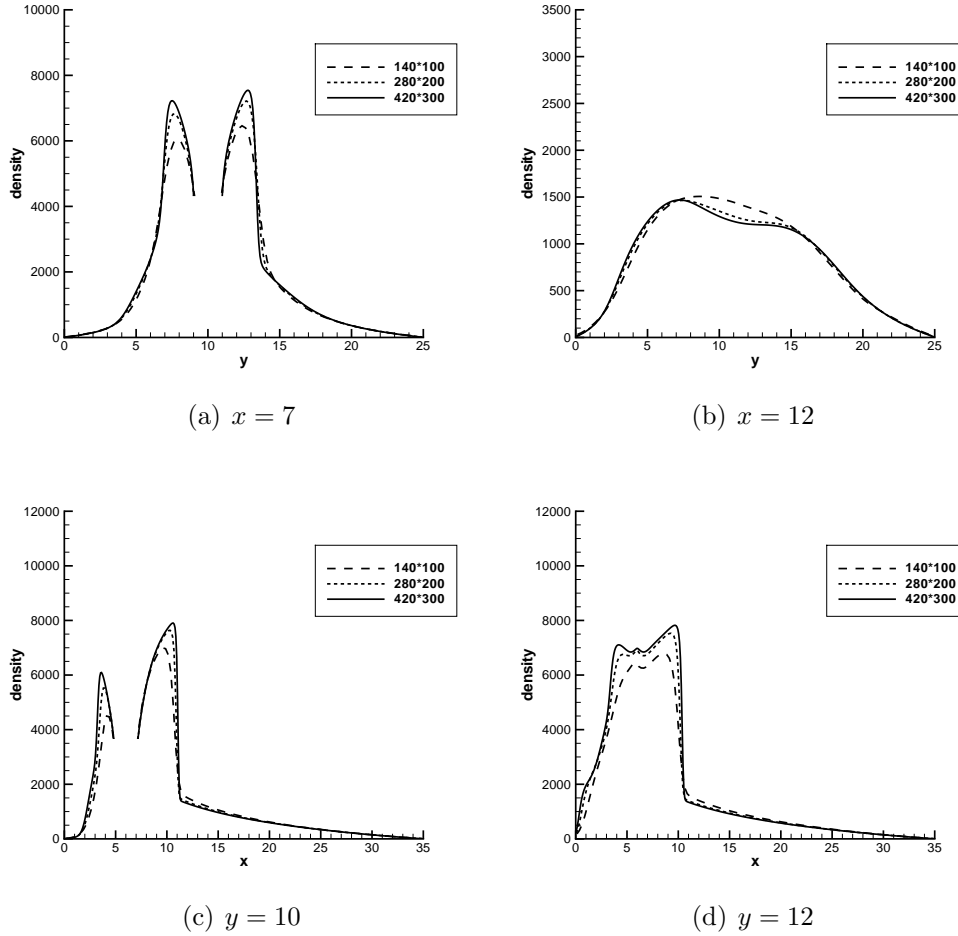
Figure 8: **Convergence curves of the density at time $t = 2$**

Figure 9 shows the temporal and spatial distributions of the density ρ within the modeling region. As Sub-figure 9(a) shows, the density is low at the beginning and the traffic is in a non-congested condition. As the traffic demand grows, the density grows. In Sub-figures 9(b) and 9(c), we can see that the density of the region near the CBD exceeds the critical density and the traffic becomes congested. We can also observe that the density of the region that is very close to the CBD is lower than that of the outer region. The inflow into the CBD maintains the maximum flow intensity as long as the traffic condition at the CBD boundary is congested. Although the demand starts to decrease from $t = 2$, the areas around the CBD are still in the congested condition at $t = 3$ due to limitations on the maximum flow intensity into the CBD (Sub-figure

9(d)). As the demand decreases further, all parts of the city return to the non-congested condition (Sub-figure 9(f)).

Figure 10 illustrates the contours of the total cost potential function ϕ at various times. At the beginning of the modeling period, when the density is very low, the distribution of the contours is uniform. As the traffic demand grows, the total cost potential increases. From the density results, we know that the density around the CBD is very high when $t = 2.5$ and $t = 3$. Hence, the travel cost around the CBD increases rapidly, resulting in a denser set of cost potential contours in this region (see Sub-figures 10(c) and 10(d)). As the traffic demand decreases, the traffic tends to enter a free-flow state and the cost potential contours tend to follow a series of concentric ellipses located around the CBD, as shown in Sub-figure 10(f). The shape of the ellipses represents the anisotropism of the model.

Figure 11 shows the plots of the flow vector, which illustrates the results of the path choice. When the density of the region around the CBD increases, vehicles choose a curved trajectory to avoid this region. This demonstrates the capability of the proposed PDUE-C model in modeling how travelers alter their preferred routes in response to dynamic changes in the network conditions to minimize their cost potentials. At the end of the modeling period, when the density is low, vehicles move toward the CBD in almost straight lines.

Consider the total inflow to the CBD through Γ_c, defined as

$$f_{CBD}(t) = \oint_{\Gamma_c} (\mathbf{F} \cdot \mathbf{n})(x, y, t) ds, \tag{83}$$

where $\mathbf{n}$ is the unit normal vector pointing toward the CBD, and the total demand over the whole domain defined as

$$q_\Omega(t) = \int \int_\Omega q(x, y, t) dx dy. \tag{84}$$

Figure 12 shows the relationship between $f_{CBD}(t)$ and $q_\Omega(t)$. The numerical data show that the areas under these two curves are the same, which demonstrates that all of the
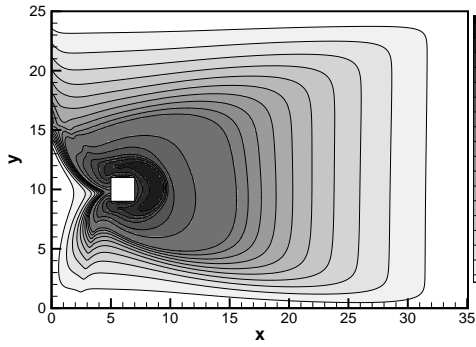
(a) $t = 1.5$
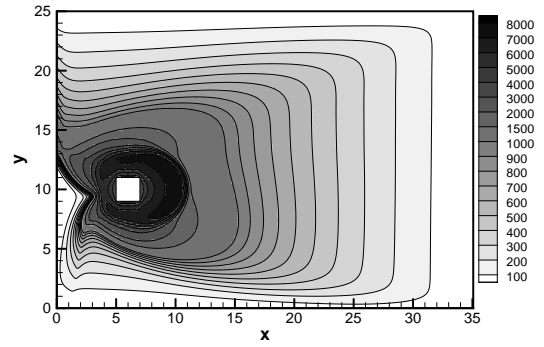
(b) $t = 2.0$
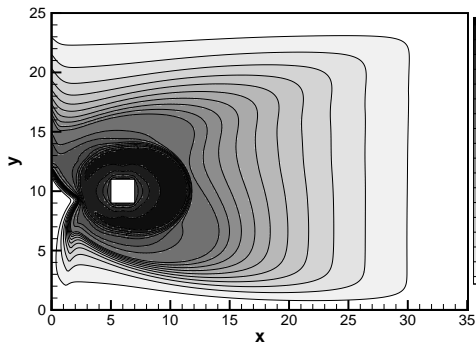
(c) $t = 2.5$
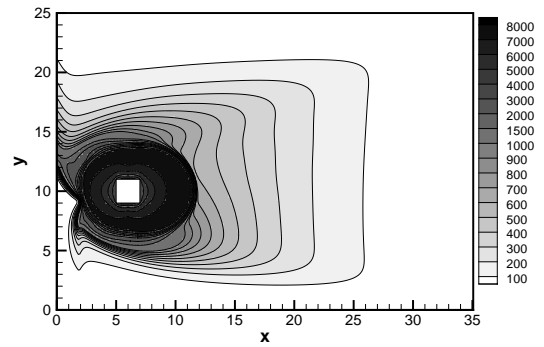
(d) $t = 3.0$
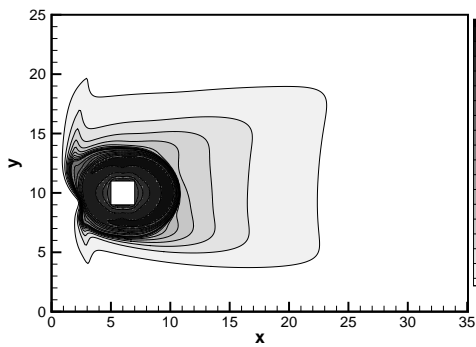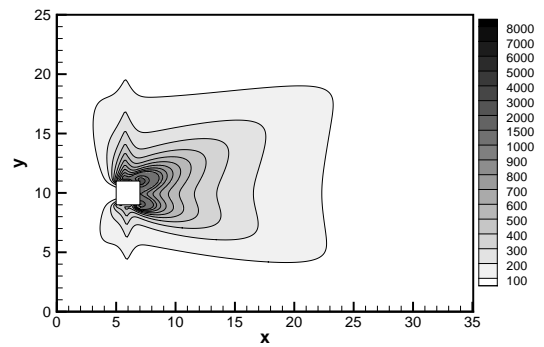
(e) $t = 3.5$

(f) $t = 5.0$

Figure 9: **Density plot**
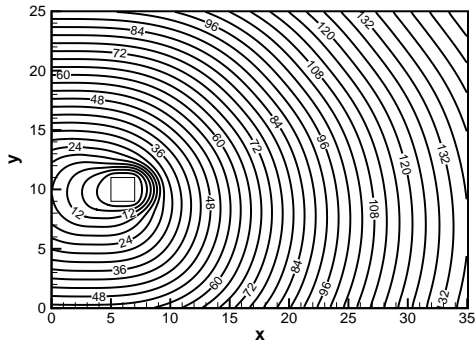
(a) $t = 1.5$
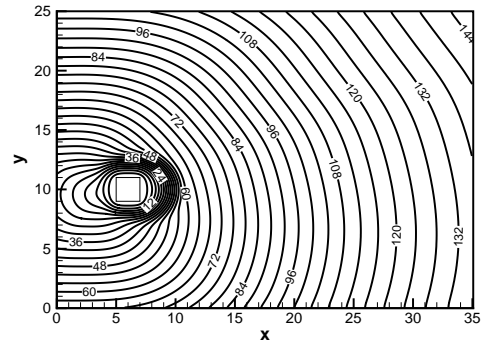
(b) $t = 2.0$
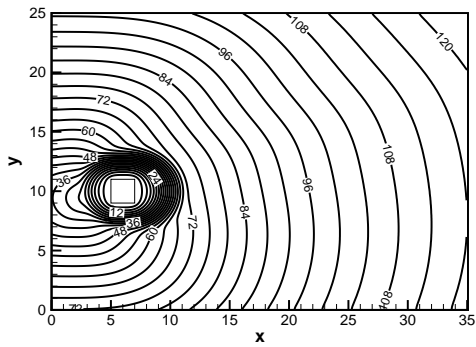
(c) $t = 2.5$
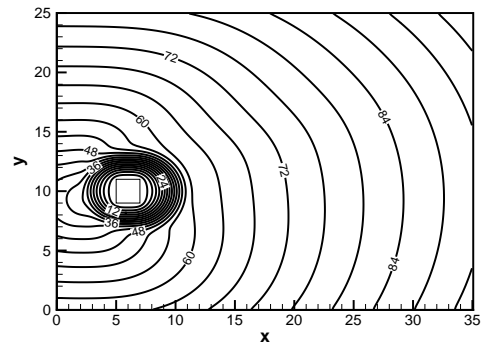
(d) $t = 3.0$
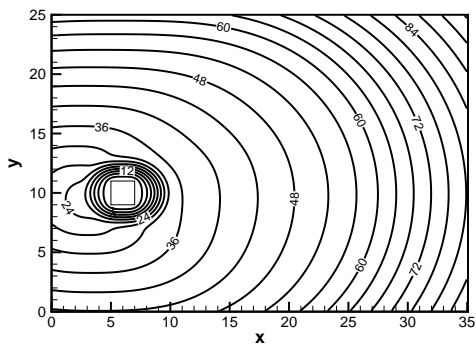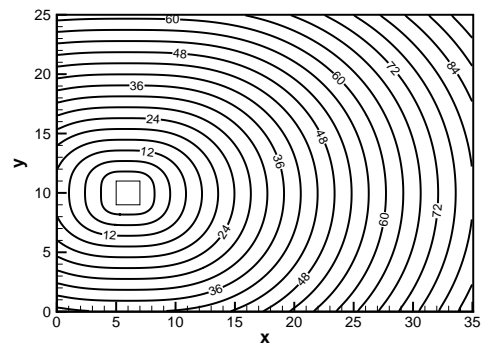
(e) $t = 3.5$

(f) $t = 5.0$

Figure 10: **Cost potential plot**
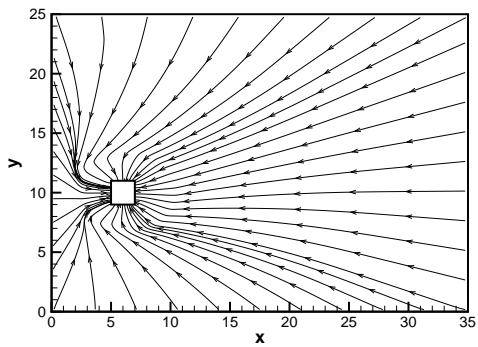
36
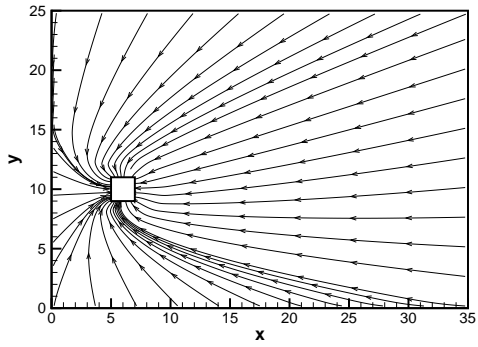
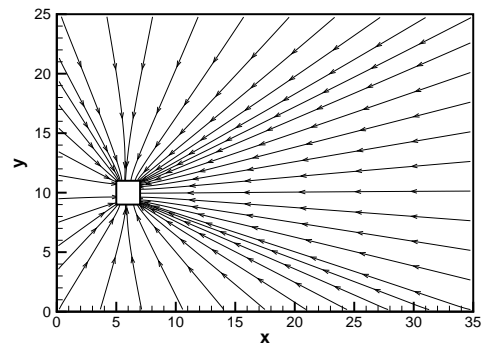(a) $t = 1.5$ (b) $t = 2.0$
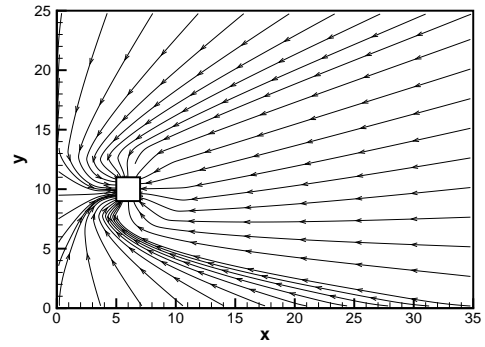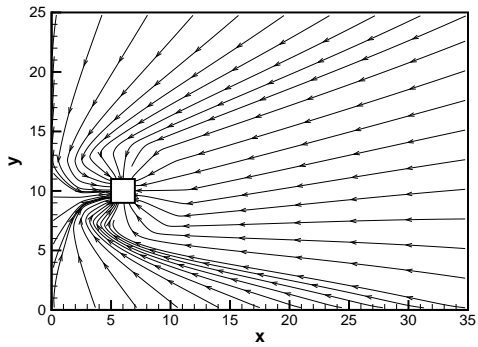
(c) $t = 2.5$ (d) $t = 3.0$
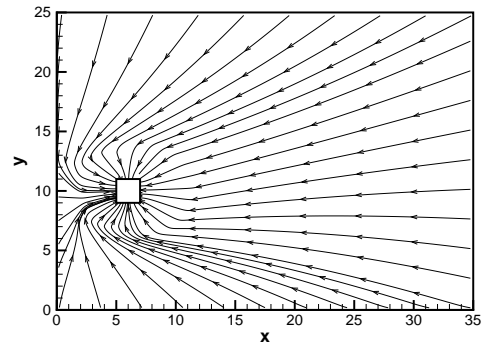
(e) $t = 3.5$ (f) $t = 5.0$

Figure 11: **Flow vector plot**

37

traffic has entered the CBD by the end of the modeling period. The inflow to the CBD increases rapidly at the beginning because the demand $q_\Omega(t)$ grows. $f_{CBD}(t)$ reaches the maximum value quickly. This means that the density around the CBD boundary is now greater than the critical density ρ_c and the traffic is in a congested condition. The inflow does not increase further due to limitations on the maximum flow intensity. The inflow to the CBD maintains this maximum value, and does not decrease until the density around the CBD decreases below ρ_c. When the traffic demand starts to decrease from $t = 2$, it takes a while to return to the non-congested condition, and the inflow then begins to fall. Note that the total demand becomes a constant (> 0) at $t = 3$, and that the inflow decreases to the same constant after a short delay. The traffic demand falls to 0 after $t = 5h$, and the flow intensity decreases to 0 thereafter.
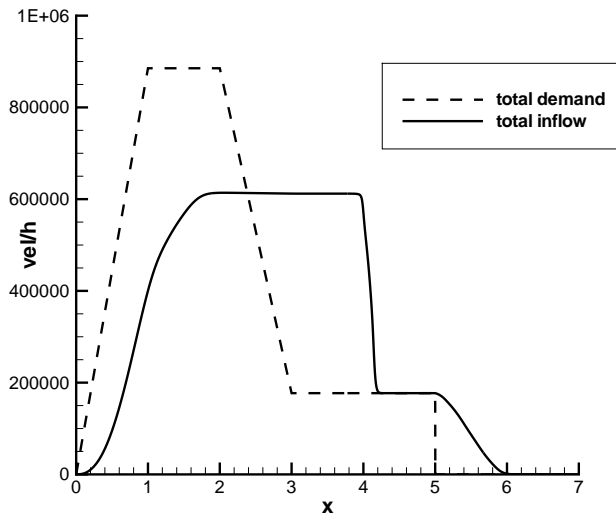
Figure 12: Flow intensity over time

Figure 13 shows the one-dimensional cuts of the speed intensity $U = U_f G(\rho)$ along the line $x = 3$ at different times. At the beginning of the modeling period, the density is low and the speed is almost the free-flow speed $U_f = u_f h(\xi)$. Although $u_f(3, y)$ is smaller in the region closer to the CBD (near $y = 10$), where there are more junctions,

the free-flow speed U_f is faster in this region because the travel direction is pointing to the east (see Figure 11) and hence $h(\xi)$ in this region is bigger. This demonstrates the anisotropy property of our model. From Figure 9, we know that the density around the CBD increases soon and hence $G(\rho)$ becomes small. We can see that the speed variation dramatically impact the shape of the speed plot and the speed becomes slower near $y = 10$ (see Sub-figures 13(d)-13(f)). As the density decreases after $t = 3.5$, the speed returns to the free-flow speed.

| (a) $t = 1.0$ | (b) $t = 1.5$ | (c) $t = 2.0$ |

| (d) $t = 2.5$ | (e) $t = 3.0$ | (f) $t = 3.5$ |

| (g) $t = 4.0$ | (h) $t = 5.0$ | (i) $t = 7.0$ |
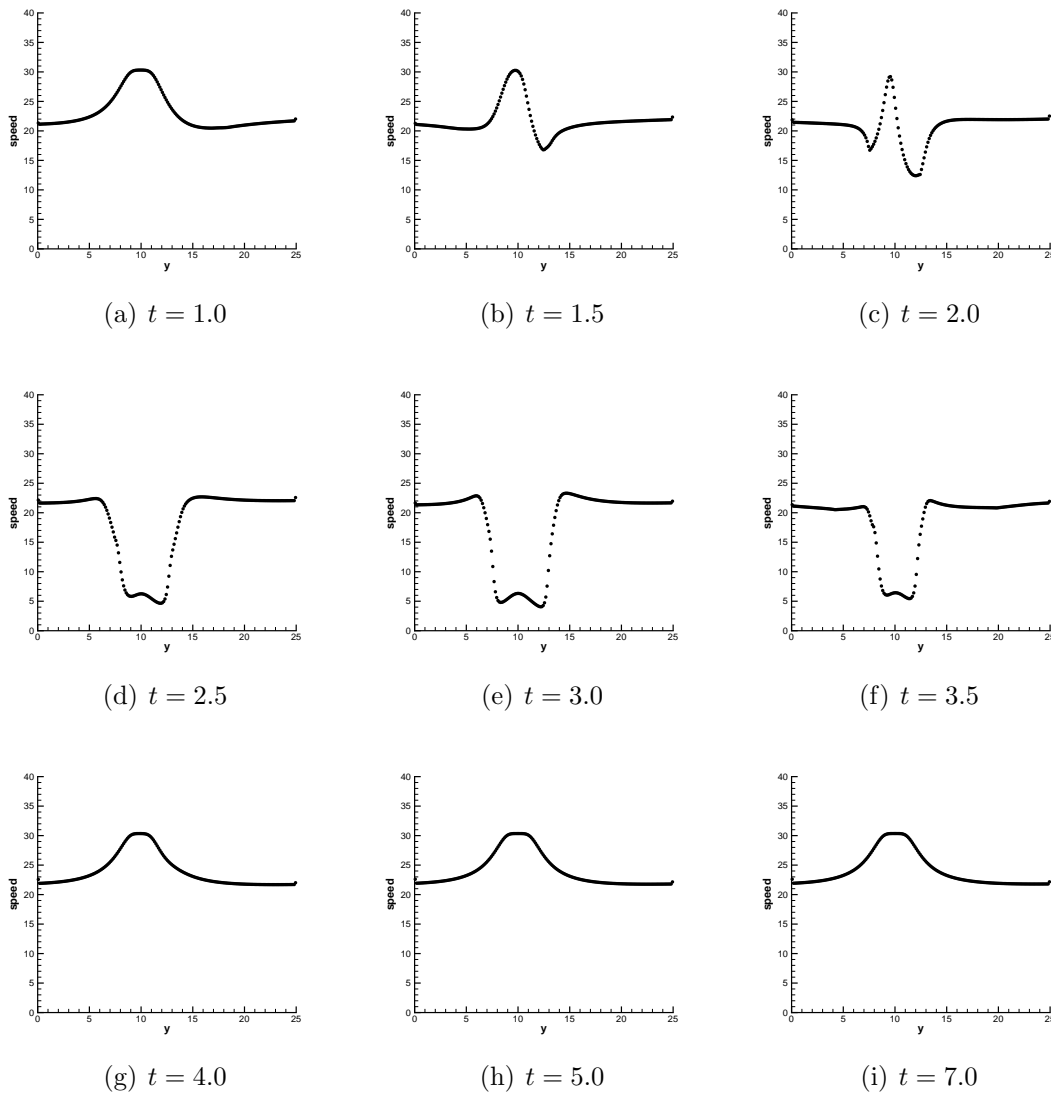
Figure 13: **one-dimensional cuts of the speed at** $x = 3$

Figure 14 shows the one-dimensional cuts of the speed intensity along the line $y = 12$

39

at different times. The region around $x = 6$ is closer to the CBD and hence have smaller u_f. Also, the flux vector in this region points to the south direction and hence have smaller $h(\xi)$. Therefore, the free-flow speed $U_f = u_f h(\xi)$ is slower around $x = 6$ (see Sub-figures 14(a) and 14(i)). As the density around the CBD grows, the speed there decreases rapidly and we can observe a significant speed jump around $x = 10$. This jump moves from the left side of $x = 10$ to the right side as the high density area around the CBD becomes larger (see Sub-figures 14(b) to 14(e)). This demonstrates the wave propagation of speed.

(a) $t = 1.0$ (b) $t = 1.5$ (c) $t = 2.0$

(d) $t = 2.5$ (e) $t = 3.0$ (f) $t = 3.5$

(g) $t = 4.0$ (h) $t = 5.0$ (i) $t = 7.0$
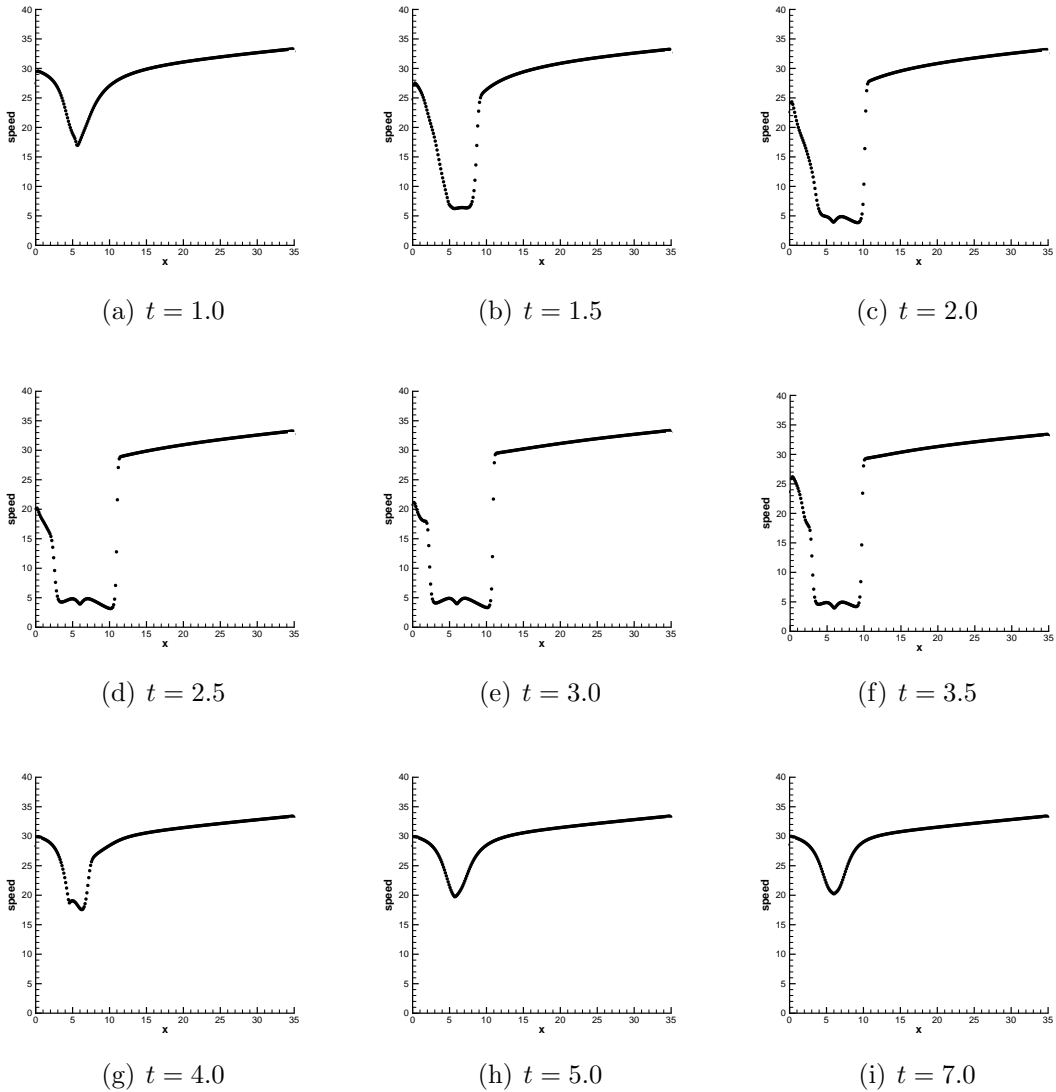
Figure 14: **one-dimensional cuts of the speed at** $y = 12$

6.1.3 Comparison with the isotropic case

By deleting the anisotropic item $h(\xi(x,y,t)) = [\cos(2\xi)+5]/6$ from the expression of the speed $U(x,y,t)$, we define an isotropic speed function $V(x,y,t)$ as follows:

$$V(x,y,t) = u_f(x,y)G(\rho) = U_{max}[1 + \gamma_2 d(x,y)]G(\rho). \tag{85}$$

By replacing $U(x,y,t)$ with $V(x,y,t)$, the model now becomes isotropic. In this case, the optimal travel direction is $\mathbf{v} \parallel -\nabla\phi$.

Figure 15 shows the comparison of the isotropic and anisotropic cases at $t = 3$. Because the traffic characteristics are uniform in all orientations for the isotropic case, the contours of the density and the cost tend to be circles (see Figures 15(a) and 15(c)). For the anisotropic condition, the factor $[\cos(2\xi) + 5]/6$ expresses the faster free-flow speed in the east-west direction. Hence, the contours tend to be ellipses with the major axis parallel to the x-axis (see Figures 15(b) and 15(d)).

By comparing Figures 15(e) and 15(f), we can see that the travelers for both cases will choose the curved path to the CBD to avoid the high density region. However, the travelers for the anisotropic case will choose a more circuitous path. The travelers coming from the east side will even travel to the west side of the CBD first and turn back due to the faster travel speed in the east-west direction.

6.2 Multiple CBDs
6.2.1 Problem setting

As shown in Figure 16, we consider a rectangular computational domain with two CBDs. The center of CBD 1 is located at (6 km, 10 km). The center of CBD 2 is located at (30 km, 15 km). The traffic demand function of Group m ($m = 1,2$) is

$$q^m(x,y,t) = q_{max}[1 - \gamma_1 d^m(x,y)]s(t), \tag{86}$$

where $d^m(x,y)$ is the distance from location (x,y) to the center of CBD m. q_{max}, γ_1 and $s(t)$ remain the same as in the previous example. The free-flow speed of Group m
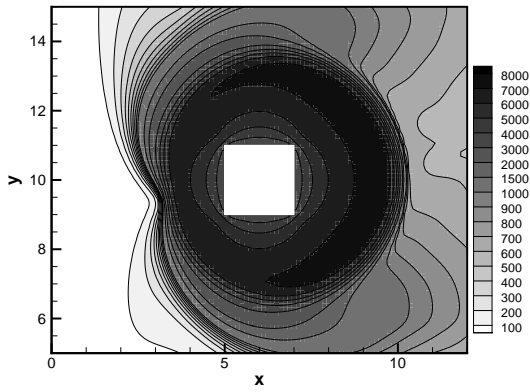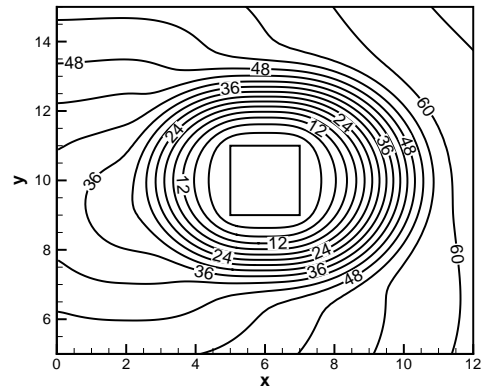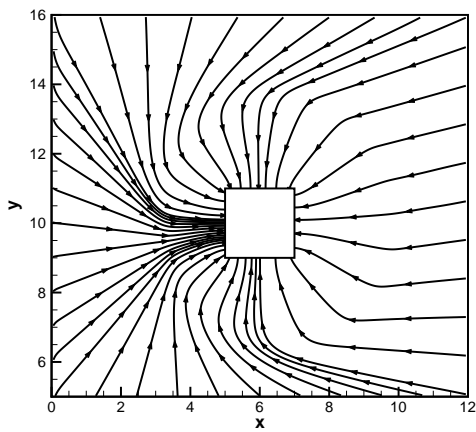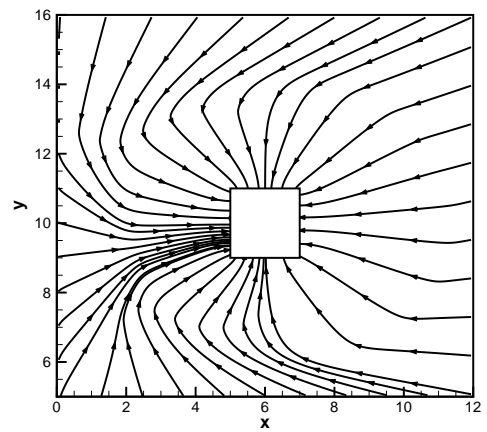
(a) density, isotropic
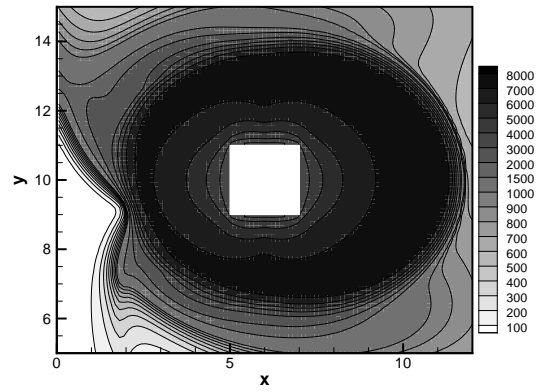
(b) density, anisotropic
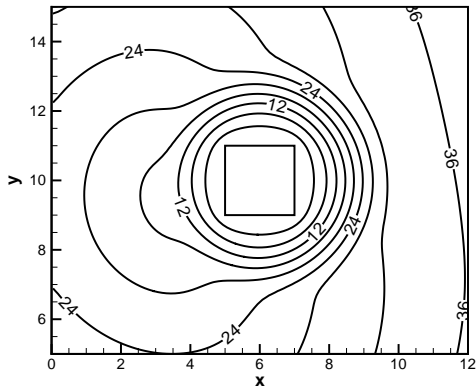
(c) cost potential, isotropic

(d) cost potential, anisotropic

(e) flow vector, isotropic

(f) flow vector, anisotropic

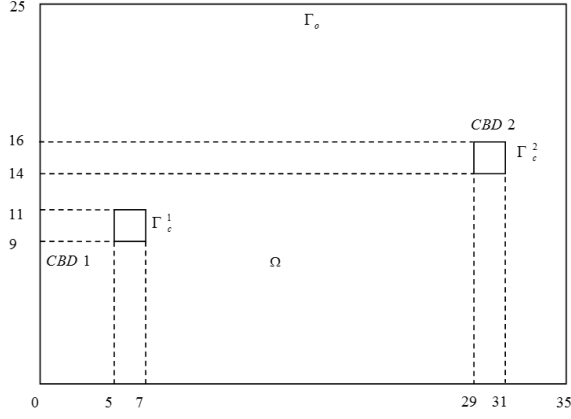Figure 15: **Comparison at** $t = 3.0$

Figure 16: The modeling domain with two CBDs

is defined as

$$U_f^m(x, y, t) = U_{max}[1 + \gamma_2 d(x, y)]h(\xi^m(x, y, t)). \qquad (87)$$

The factor $[1 + \gamma_2 d(x, y)]$ is used to express the faster free-flow speed in the domain with larger $d(x, y)$. Here, we define $d(x, y) = \frac{3}{4}\min\{d^1(x, y), d^2(x, y)\} + \frac{1}{4}\max\{d^1(x, y), d^2(x, y)\}$ which shows that the impact of the closer CBD is more crucial. However, we need also consider the influence of the farther CBD. $G(\rho)$ and all other functions are the same as in the previous example.

For Group m, the numerical boundary conditions at the outer boundary of the city and the boundary of the mth CBD are the same as in the previous example. The boundaries of CBDs other than the mth CBD (Γ_c^n, $n \neq m$) are viewed as solid walls for Group m. The numerical boundary conditions on these solid walls are the same as the outer boundary of the city (Γ_o), that is, we let the normal numerical flux of Group m be 0 and set $\rho^m = 0$ at the ghost points inside the wall. In the HJ equation, ϕ^m at the ghost points are obtained by extrapolation from inside the computational domain.

6.2.2 Numerical results

Let us consider the convergence of self-adaptive MSA for both the previous example with one single CBD and the example in this section with two CBDs. Figure 17 shows

43

the step size sequences λ_k. Figure 18 shows the errors of ϕ between each iteration, i.e., $\|\vec{\phi}^{k+1} - \vec{\phi}^k\|$. The results of both examples are similar. For the first several iterations, the predetermined step sizes decrease fast, avoiding too large an amplification of the error. We can see that the errors increase at the very beginning and then decrease rapidly. After a number of iterations, the step sizes decrease slowly and trend toward the optimal step size, and the errors decrease at a reasonable speed.
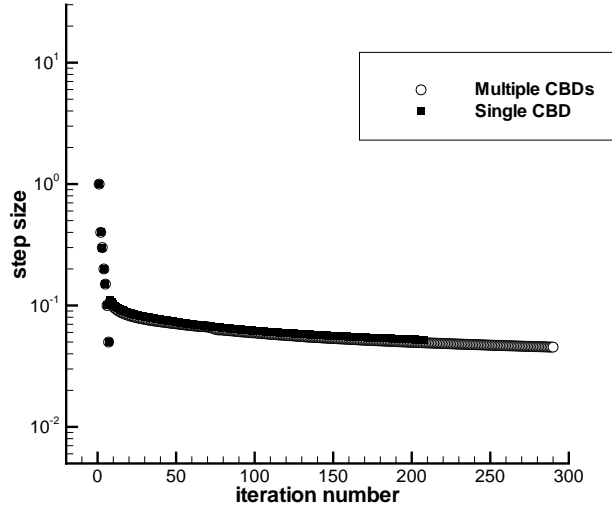
Figure 17: The step sizes of the self-adaptive MSA

Figures 19 to 21 show the plots of the density, cost potential and flow vector, respectively. The results are similar as in the example with one single CBD. As the traffic demand of each group grows, the density around each CBD increases and the traffic becomes congested, resulting in a denser set of cost potential contours around each CBD. Also, the flow vector of each group becomes curved to avoid high density region. As the density decreases at the end of the time period, the traffic reverts back to the free-flow state and the cost potential contours tend to follow a series of concentric ellipses. Also, the vehicles of each group move toward the CBD in almost straight lines.

The empirical observation in Geroliminis and Daganzo (2008) show that a macro-
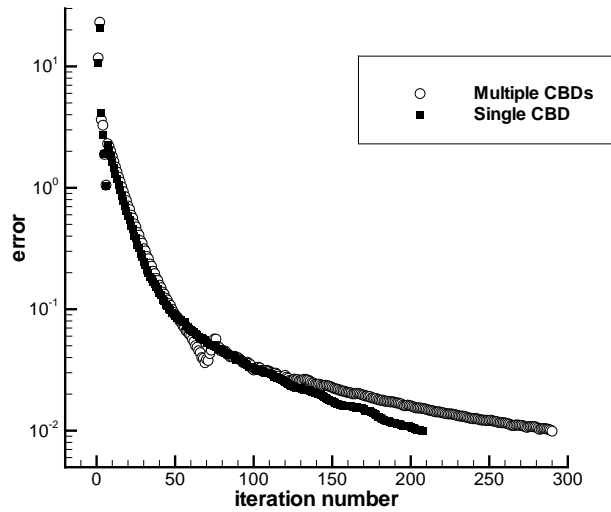
44

Figure 18: The errors of the self-adaptive MSA

scopic fundamental diagram (MFD) linking space-mean flow and density exists on a homogeneous (low spatial variance of link density) urban area independently of the demand. However, heterogeneity distribution of density can affect the shape or even the existence of MFD (Geroliminis and Sun, 2011; Daganzo et al., 2011). In Figure 22(a), we plot the relationship between the average flow and the average density of the entire city. We can observe high scatter due to the heterogeneously distributed congestion. Mazloumian et al. (2010) show that MFD remains well-defined in sub-regions of the urban network. Hence, the heterogeneous networks might be partitioned into a small number of more homogenous regions so that each region will have a well-defined MFD. See Ji and Geroliminis (2012) for a partitioning mechanism. Note that MFD is an important attempt to model a dense urban network. Gayah and Daganzo (2011) investigate the effect of driver adaptation and route choice on the shape of MFD. Yildirimoglu and Geroliminis (2014) incorporate the MFD framework into a DTA model and establish dynamic equilibrium conditions in case of heterogeneous urban networks. Ramezani et al. (2015) introduce two aggregated models, region- and subregion-based MFDs, to study
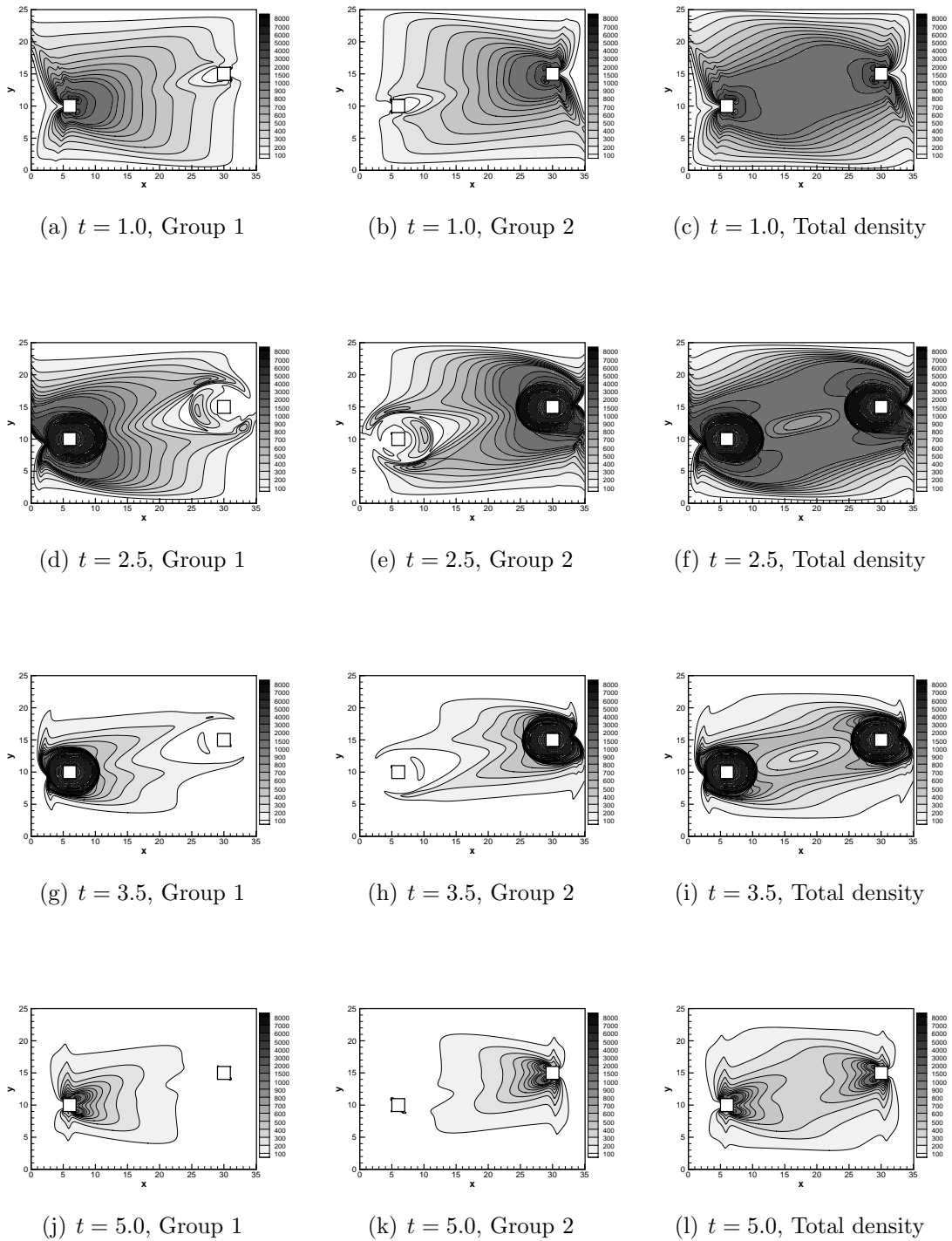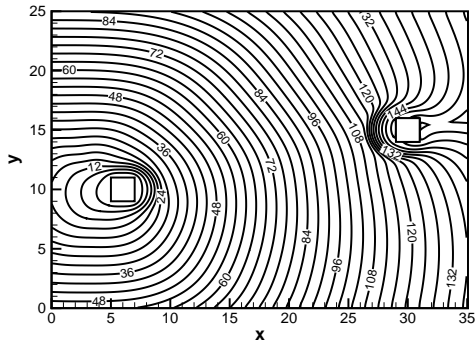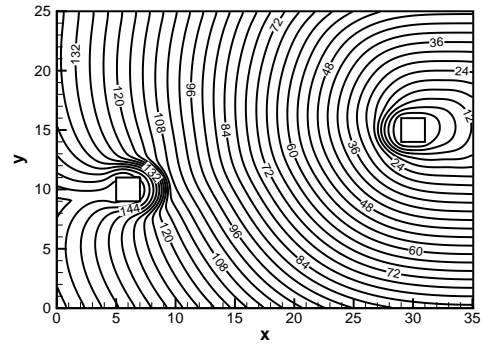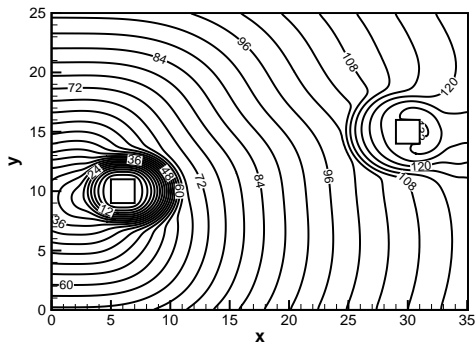
(a) $t = 1.0$, Group 1　　　(b) $t = 1.0$, Group 2　　　(c) $t = 1.0$, Total density

(d) $t = 2.5$, Group 1　　　(e) $t = 2.5$, Group 2　　　(f) $t = 2.5$, Total density

(g) $t = 3.5$, Group 1　　　(h) $t = 3.5$, Group 2　　　(i) $t = 3.5$, Total density

(j) $t = 5.0$, Group 1　　　(k) $t = 5.0$, Group 2　　　(l) $t = 5.0$, Total density
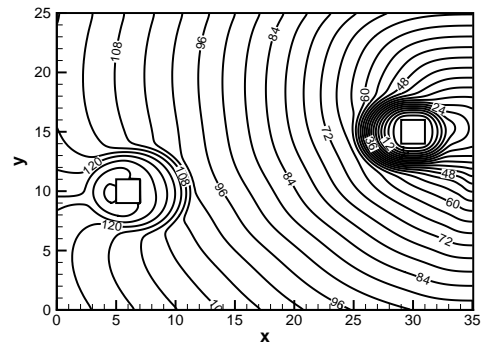
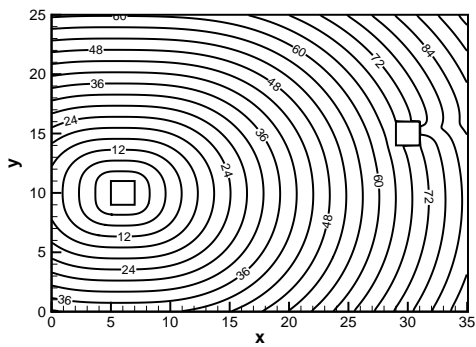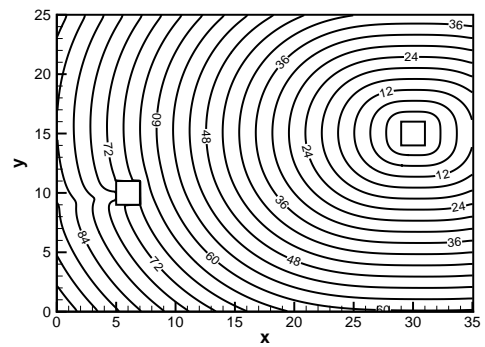Figure 19: **Density plot of Multiple CBDs**

(a) $t = 1.5$, Group 1

(b) $t = 1.5$, Group 2
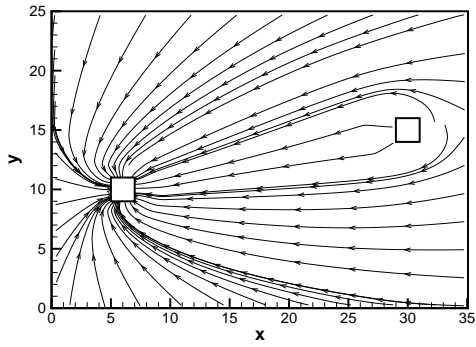
(c) $t = 2.5$, Group 1

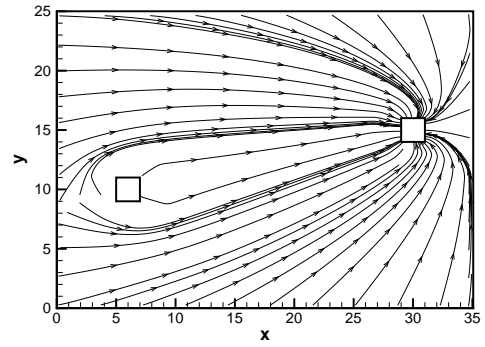(d) $t = 2.5$, Group 2

(e) $t = 5.0$, Group 1
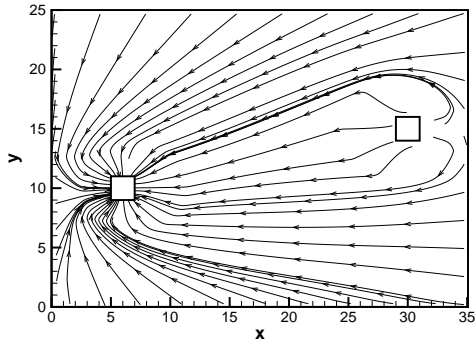
(f) $t = 5.0$, Group 2

Figure 20: **Cost potential plot of Multiple CBDs**
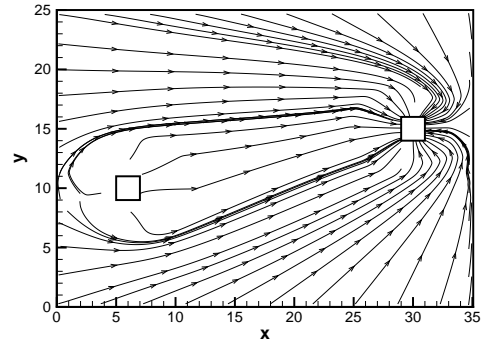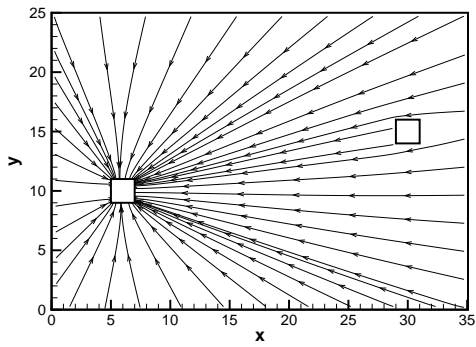
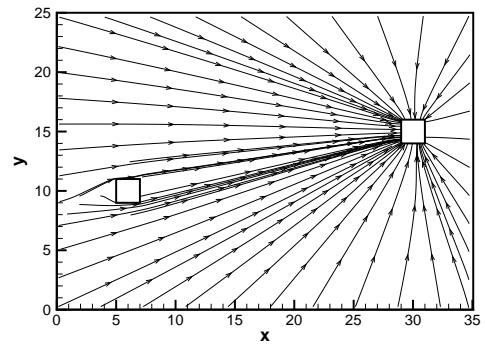(a) $t = 1.5$, Group 1

(b) $t = 1.5$, Group 2

(c) $t = 2.5$, Group 1

(d) $t = 2.5$, Group 2

(e) $t = 5.0$, Group 1

(f) $t = 5.0$, Group 2

Figure 21: **Flow vector plot of Multiple CBDs**

the dynamics of heterogeneity and how they can affect the accuracy scatter and hysteresis of a multi-subregion MFD model. We now show that our model is able to reproduce the MFD plots for homogenous sub-regions. Figure 22(b) shows two scattered plots in a square sub-region near CBD 1 which is centered at $(6km, 13km)$ and with side lengths of 0.25 km (circle symbols) and 0.50 km (square symbols). We can see that both cases exhibit similar MFDs, but the MFD associated with the larger sub-region with a high degree of heterogeneity becomes more scattered, which are consistent with the above literatures.

7   Conclusions

In this paper, we reformulate the model constructed in Hoogendoorn and Bovy (2004). Their model consists of a CL and an HJB equation, and each contains a minimum value problem. The HJB is difficult to compute in most anisotropic cases. The authors of Hoogendoorn and Bovy (2004) did not offer a numerical algorithm to solve the minimum value problem in the HJB equation for anisotropic cases, and only provided an isotropic application example in their paper. To overcome this problem, we reformulate their model for a dense polycentric urban city with multiple CBDs. When we compute the
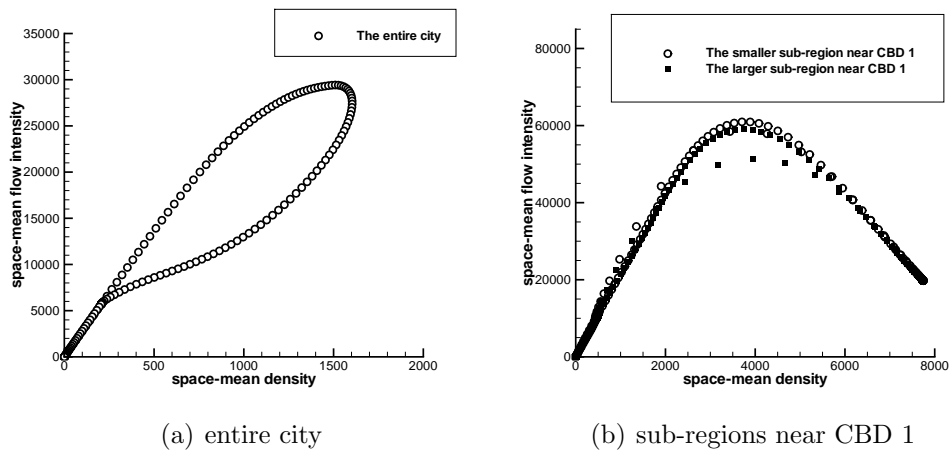

(a) entire city   (b) sub-regions near CBD 1

Figure 22: **MFD plots**

49

actual cost, the velocity vector is known, and hence the HJB equation reduces to a HJ equation that includes no minimum value problem and is much easier to compute. In our model, the minimum value problem is used only in the CL portion. Hence, the computation of our model is simpler. Also, there is only one parameter in the numerical scheme of the minimum value problem in our model under the assumption that the cost is only related to the time, whereas there are still four parameters in Hoogendoorn and Bovy (2004). Hence, the minimum value problem in our model is easier to compute. A simple algorithm is given in this paper to solve this minimum value problem. We only need to solve the minimum value problem in advance rather than solving it again during the iterative solution process. We also prove the dynamic path equilibrium of our model in a different way. Two anisotropic numerical examples are shown to demonstrate the effectiveness of the model and the solution algorithm.

Although the model is composed for a general cost function, we only show how to compute the minimum value problem under the assumption that the cost is only related to the time. The solution algorithm for a general cost needs to be considered in the future. In this paper, we develop a numerical scheme based on a rectangular grid. It would be useful to extend the numerical scheme based on a triangular grid system, which is more flexible for tackling complicated geometry. Extensions such as a combined departure time and assignment could be developed in future studies.

Daganzo and Geroliminis (2008) and Geroliminis and Boyaci (2012) analytically explore the connection between network structure (e.g., topology and signal control) and a network's MFD for urban cities. Leclercq and Geroliminis (2013) study the influence of route choice in the MFD for a network of parallel routes under different traffic conditions, static and dynamic case for user equilibrium and system optimum. In our case, we would be able to change the shape of MFD though controlling the parameters in the problem setting. Efficient traffic management of large-scale urban areas is of great importance. Well-defined MFDs are very useful to introduce control strategies to improve

mobility in large urban networks such as those in Aboudolas and Geroliminis (2013); Daganzo (2007); Geroliminis et al. (2013); Haddad et al. (2013); Keyvan-Ekbatani et al. (2013, 2015). The dynamic continuum model presented in our paper offers an alternative approach to the study of this interesting problem. As our model is able to reproduce low-scatter MFDs for sub-regions, we may try to perform a similar control in the future work. Although it may be difficult to directly apply the same in our paper, these strategies are also possible for our case through controlling the parameters such as optimizing the signal timings of the junctions that would be able to change the shape of the MFD.

For the case of discrete modeling, the existence of DUE for car traffic has been analyzed by several papers (Bressan and Han, 2013; Han et al., 2013; Zhu and Marcotte, 2000). For the continuous model described in this paper, the existence of DUE might be considered from the perspective of the existence of solution to the PDEs describing the model. Our model consists of two coupled PDEs (CL and HJ) with forward-backward structure. This model is similar to mean field models in finite horizon (Lasry and Lions, 2006, 2007) which are also systems of two coupled PDEs with forward-backward structure. The existence theorems of the solutions to mean field models under suitable assumptions can be found in Cardaliaguet et al. (2012), Lasry and Lions (2006) and Lasry and Lions (2007). Although our model is not exactly the same as the mean field models, we can investigate the existence of DUE using the idea in the above papers in our future work.

Acknowledgements

References

Aboudolas, K., Geroliminis, N., 2013. Perimeter and boundary flow control in multi-reservoir heterogeneous networks. Transportation Research Part B 55, 265–281.

Bar-Gera, H., Boyce, D., 2006. Solving a non-convex combined travel forecasting model by the method of successive averages with constant step sizes. Transportation Research Part B 40 (5), 351–367.

Bellman, R., 1957. Dynamic Programming. Princeton University Press, Princeton, New Jersey.

Boyce, D.E., Ran, B., Leblanc, L.J., 1993. Solving an instantaneous dynamic user-optimal route choice model. Transportation Science 29 (2), 128–142.

Bressan, A., Han, K., 2013. Existence of optima and equilibria for traffic flow on networks. Networks and Heterogeneous Media, 8 (3), 627–648.

Buckley, D.J., 1979. Traffic assignment in a two-dimensional continuous representation of a traffic network with flow-dependent speeds. Transportation Research Part B 13 (2), 167–179.

Cardaliaguet, P., Lasry, J.-M., Lions, P-L., Porretta, A., 2012. Long time average of mean field games. Networks and heterogeneous media 7 (2) 279–301.

Chow, A.H.F., 2009. Dynamic system optimal traffic assignment – a state-dependent control theoretic approach. Transportmetrica 5 (2), 85–106.

Daganzo, C.F., 2007. Urban gridlock: macroscopic modeling and mitigation approaches, Transportation Research Part B 41 (1), 49–62. Corrigendum. Transportation Research Part B 41 (3), 379.

Daganzo, C.F., Gayah, V.V., Gonzales, E.J., 2011. Macroscopic relations of urban traffic variables: bifurcations, multivaluedness and instability. Transportation Research Part B 45 (1), 278–288.

Daganzo, C.F., Geroliminis, N., 2008. An analytical approximation for the macroscopic fundamental diagram of urban traffic. Transportation Research Part B 42 (9), 771–781.

Du, J., Wong, S.C., Shu, C.-W., Xiong, T., Zhang, M., Choi, K., 2013. Revisiting Jiang's dynamic continuum model for urban cities. Transportation Research Part B 56, 96–119.

Fleming, W.H., Soner, H.M., 1993. Controlled Markov Processes and Viscosity Solutions. Springer-Verlag.

Friesz, T.L., Bernstein, D., Smith, T., Tobin, R., Wie, B., 1993. A variational inequality formulation of the dynamic network user equilibrium problem. Operations Research 41 (1), 80–91.

Friesz T.L., Han, K., Neto, P.A., Meimand, A., Yao, T., 2013. Dynamic user equilibrium based on a hydrodynamic model. Transportation Research Part B 47 (1), 102–126.

Gayah, V.V., Daganzo, C.F., 2011. Clockwise hysteresis loops in the macroscopic fundamental diagram: an effect of network instability. Transportation Research Part B 45 (4), 643–655.

Geroliminis, N., Boyaci, B., 2012. The effect of variability of urban systems characteristics in the network capacity. Transportation Research Part B 46 (10), 1607–1623.

Geroliminis, N., Daganzo, C.F., 2008. Existence of urban-scale macroscopic fundamental diagrams: some experimental findings. Transportation Research Part B 42 (9), 759–770.

Geroliminis, N., Haddad, J., Ramezani, M., 2013. Optimal Perimeter control for two urban regions with macroscopic fundamental diagrams: a model predictive approach. IEEE Transactions on Intelligent Transportation Systems 14 (1), 348–359. http://dx.doi.org/10.1109/TITS.2012.2216877, ISSN 1524-9050.

Geroliminis, N., Sun, J., 2011. Properties of a well-defined macroscopic fundamental diagram for urban traffic. Transportation Research Part B 45 (3), 605–617.

Haddad, J., Ramezani, M., Geroliminis, N., 2013. Cooperative traffic control of a mixed network with two urban regions and a freeway. Transportation Research Part B 54, 17–36.

Han, K., Friesz, T.L., Yao, T., 2013. Existence of simultaneous route and departure choice dynamic user equilibrium. Transportation Research Part B 53, 17–30.

Hoogendoorn, S.P., Bovy, P.H.L., 2004. Dynamic user-optimal assignment in continuous time and space. Transportation Research Part B 38 (7), 571–592.

Huang, L., Wong, S.C., Zhang, M.P., Shu, C.-W., Lam, W.H.K., 2009. Revisiting Hughes' dynamic continuum model for pedestrian flow and the development of an efficient solution algorithm. Transportation Research Part B 43 (1), 127–141.

Ji, Y., Geroliminis, N., 2012. On the spatial partitioning of urban transportation networks. Transportation Research Part B 46 (10), 1639–1656.

Keyvan-Ekbatani, M., Yildirimoglu, M., Geroliminis, N., Papageorgiou, M., 2013. Traffic Signal Perimeter Control with Multiple Boundaries for Large Urban Networks., 16th International IEEE Conference on Intelligent Transportation Systems.

Keyvan-Ekbatani, M., Yildirimoglu, M., Geroliminis, N., Papageorgiou, M., 2015. Multiple Concentric Gating Traffic Control in Large-Scale Urban Networks. Intelligent Transportation Systems, IEEE Transactions on, PP(99), 1–14. DOI: 10.1109/TITS.2015.2399303.

Kuwahara, M., Akamatsu, T., 2001. Dynamic user optimal assignment with physical queue for a many-to-many OD pattern. Transportation Research Part B 35 (5), 461–479.

Lasry, J.-M., Lions, P.-L., 2006. Jeux à champ moyen. ii. Horizon fini et contrôle optimal. (French) [Mean field games. ii. Finite horizon and optimal control]. Comptes Rendus Mathematique 343 (10), 679–684.

Lasry, J.-M., Lions, P.-L., 2007. Mean field games. Japanese Journal of Mathemathics 2 (1), 229–260.

Leclercq, L., Geroliminis, N., 2013. Estimating MFDs in simple networks with route choice. Transportation Research Part B 57, 468–484.

Loo, B.P.Y., Ho, H.W., Wong, S.C., 2005. An application of the continuous equilibrium modelling approach in understanding the geography of air passenger flows in a multi-airport region. Applied Geography 25, 169–199.

Lo, H.K., Szeto, W.Y., 2002. A cell-based variational inequality formulation of the dynamic user optimal assignment problem. Transportation Research Part B 36 (5), 421–443.

Lo, H.K., Szeto, W.Y., 2005. Road pricing modeling for hyper-congestion. Transportation Research Part A 39 (7–9), 705–722.

Mazloumian, A., Geroliminis, N., Helbing, D., 2010. The spatial variability of vehicle densities as determinant of urban network capacity. Philosophical Transactions of the Royal Society A: Mathematical, Physical and Engineering Sciences 368 (1928), 4627–4647.

Peeta, S., Ziliaskopoulos, A.K., 2001. Foudations of Dynamic Traffic Assignment: The Past, the Present and the Future. Networks and Spatial Economics 1, 233–265.

Ramezani, M., Haddad, J., Geroliminis, N.,2015. Dynamics of heterogeneity in urban networks: aggregated traffic modeling and hierarchical control. Transportation Research Part B 74, 1–19.

Robbins, H., Monro, S., 1951. A stochastic approximation method. Annals of Mathematical Statistics 22 (3), 400–407.

Sheffi, Y., 1984. Urban Transportation Networks: Equilibrium Analysis With Mathematical Programming Techniques. Prentice Hall, New York.

Szeto, W.Y., Lo, H.K., 2004. A cell-based simultaneous route and departure time choice model with elastic demand. Transportation Research Part B 38 (7), 593–612.

Tong, C.O., Wong, S.C., 2000. A predictive dynamic traffic assignment model in congested capacity-constrained road networks. Transportation Research Part B 34 (8), 625–644.

Vaughan, R.J., 1987. Urban Spatial Traffic Patterns. Pion, London, U.K.

Wong, S.C., 1998. Multi-commodity traffic assignment by continuum approximation of network flow with variable demand. Transportation Research Part B 32 (8), 567–581.

Wong, S.C., Lee, C.K., Tong, C.O., 1998. Finite element solution for the continuum traffic equilibrium problems. International Journal for Numerical Methods in Engineering 43 (7), 1253–1273.

Xiong, T., Zhang, M., Shu, C.-W., Wong, S.C., Zhang, P., 2011. High-order computational scheme for a dynamic continuum model for bi-directional pedestrian flows. Computer-Aided Civil and Infrastructure Engineering 26, 298–310.

Yildirimoglu, M., Geroliminis, N., 2014. Approximating dynamic equilibrium conditions with macroscopic fundamental diagrams. Transportation Research Part B 70, 186–200.

Zhang, X., Huang, H.J., Zhang, H.M., 2008. Integrated daily commuting patterns and optimal road tolls and parking fees in a linear city. Transportation Research Part B 42 (1), 38–56.

Zhu, D.L., Marcotte, P., 2000. On the existence of solutions to the dynamic user equilibrium problem. Transportation Science 34 (4), 402–414.